Research Square

Preprints are preliminary reports that have not undergone peer review.
They should not be considered conclusive, used to inform clinical practice,
or referenced by the media as validated information.

Geochemistry, mineralogy and petrogenesis of Post-collisional potassic adakitic syenites from the Lar igneous suite in the southeast of Iran: an insight into the mantle source region

Sasan GHAFARIBIJAR

sasan.ghb@sci.uk.ac.ir

Shahid Bahonar University of Kerman

Mohsen ARVIN

Shahid Bahonar University of Kerman

Sara DARGAHI

Shahid Bahonar University of Kerman

Research Article

Keywords: Lar Igneous Suite, Adakitic syenite, Metasomatized mantle, post-collision, slab melts.

Posted Date: November 12th, 2026

DOI: https://doi.org/10.21203/rs.3.rs-10576396/v1

License: This work is licensed under a Creative Commons Attribution 4.0 International License.
Read Full License

Additional Declarations: No competing interests reported.

Geochemistry, mineralogy and petrogenesis of Post-collisional potassic adakitic syenites from the Lar igneous suite in the southeast of Iran: an insight into the mantle source region

Sasan GHAFARIBIJAR[1]*, Mohsen ARVIN[1], Sara DARGAHI[1]

[1] Department of Geology, College of Science, Shahid Bahonar University of Kerman, KERMAN 76169-14111, Iran

Correspondence to: **E:** sasan.ghb@sci.uk.ac.ir

Abstract

The Lar Igneous Suite (LIS) which occurs in the central part of the Sistan suture zone, east of Iran, comprises post collisional silica-undersaturated to silica over-saturated K_2O rich rocks such as syenite, shonkinite, lamprophyres, monzonite, tuff and breccia. Geochemistry, mineralogy and petrogenesis of the syenites which represent adakitic (Sr/Y >27 and La/Yb >20) signatures have been studied here. The syenites are also shoshonitic in composition (K_2O/Na_2O=0.86 to 1.99) with variable amount of SiO_2 and MgO, as well as relatively high Al_2O_3 and low TiO_2. The LIS syenites are also enriched in LILE and LREE, fractionated in LREE/HREE and MREE/HREE, and depleted in HFSE that confirm they were derived from a refractory, re-enriched lithospheric mantle source in an orogenic setting. Based on geochemical

data, their high K_2O and K_2O/Na_2O ratio is a primary feature related to the source region; and partial melting plays the most important role in their geochemical variations. Furthermore, geochemical signatures of the LIS syenites indicate that the mantle source region experienced at least two types of metasomatic enrichment; oceanic slab-derived adakitic melts, and sediment melts that further have enriched the source region in K (most probably in the form of phlogopite crystallization). The onset of magmatism that triggered adakitic nature of the LIS syenites has occurred after Iran-Helmand micro plate collision and subsequent uplift in the Sistan suture zone. Subsequently, partial melting of the metasomatized subcontinental lithospheric mantle has produced hybrid magmas which inherited geochemical signatures of both refractory peridotite and re-fertilized portions.

Keywords

Lar Igneous Suite, Adakitic syenite, Metasomatized mantle, post-collision, slab melts.

Introduction

The term ‘adakite’ was initially defined by Defant and Drummond (1990) for rocks with high Sr/Y and La/Yb ratios derived by melting of basaltic portion of the subducted oceanic crust. Significantly, such geochemical features are also achieved via different petrogenetic processes in a variety of tectonic settings; these petrogenetic processes may be divided into three groups; (1) partial melting of a thickened mafic lower-crust (Atherton and Petford, 1993; Hou et al., 2004), (2) partial melting of a delaminated lower continental crust (Gao et al., 2004; Wang et al., 2007), and (3) magma assimilation and fractional crystallization (AFC) of basaltic melts (Castillo et al., 1999; Macpherson et al., 2006). Among the numerous adakites and/or adakitic

rocks that have been investigated, the continental adakitic rocks have caused some confusion and debates; despite being geochemically similar to the modern slab-derived adakites, most continental adakitic rocks are K-rich. On the other hand, high potassium magmatism in post orogenic settings are believed to have been generated by following processes, (1) low-degree partial melting of a source with low K_2O contents at high pressures such as lower continental crust (Rapp *et al*., 2002; Huang and He, 2010), (2) partial melting of a metasomatized mantle source with high K_2O contents (Rapp *et al*., 2002), and (3) fractional crystallization (Pla Cid et al., 2000; Brotzu et al., 2007).

The Lar Igneous Suite (LIS) that is located in the north of Zahedan, east of Iran, is defined by post-collisional, high-K adakitic magmatism (Ghafaribijar, 2010). Due to these geodynamic and geochemical features, the nature of the LIS magma sources has been a topic of debate. In this study, we report new petrographic, mineralogic and geochemical data from the syenitic rocks in the Lar Igneous Suite. Our data show that the adakite-like signatures (e.g., high Sr/Y and La/Yb ratios) and K-enrichment in these rocks have been primarily generated by partial melting of a mantle source region metasomatized by hybrid subducted oceanic slab melts and sediment melts, rather than of partial melting in a thickened lower crust and or fractional crystallization of mantle-derived melts.

Geological setting

The Afro-Arabian collision zone and the central part of the Tethyan belt which now occupied by Iran, Turkey, and western Pakistan is made up of a collage of island arcs and continental fragments originally rifted from the northern margin of Gondwana. The main Neotethyan Ocean expanded when the Sanandaj–Sirjan Zone and Central Iranian microcontinent (Lut and Tabas blocks) rifted from the northeastern margin of Gondwana in the Early Triassic (Hooper

et al., 1994). By the Late Triassic or Early Jurassic these continental fragments had collided with the southern margin of Eurasia, and northward-directed subduction of the Neotethys Ocean began beneath this accreted margin (Horton et al., 2008). Rifting (maybe back arc rifting) along the accreted margin opened several small ocean basins such as the Sabzevar and Sistan oceans in northeast and eastern Iran, respectively (Richards, 2015). The Neotethys subduction continued until the subsequent continental collision between Arabia and Eurasia accompanied by the closure of the Neotethys and the small ocean basins (Sabzevar and Sistan oceans) in Late Cretaceous to Oligocene-Miocene. As a result of the Afro-Arabian collision, three mountain ranges developed in Iran: (a) Alborz–Kopeh Dagh in the north, (b) Zagros orogenic belt in the southwest and (c) East Iranian ranges in the east (Fig. 1a; Pang et al., 2013). They are marked respectively by Paleotethyan suture along southern edge of the Alborz–Kopeh Dagh (Alavi et al., 1997), and Neotethyan suture zones that include the Bitlis–Zagros in southwest of Iran (Agard et al., 2011 and references therein) and Sistan suture in eastern Iran (Fig. 1a) (McCall, 1997).

The N-S trending Sistan suture zone has been developed in three stages (Chance, 1981): (1) the formation of oceanic crust west of the Helmand (Afghan) micro-continent that led subsequently to deposition of volcano-clastics during Late Cretaceous to Paleocene, (2) deposition of shallow marine carbonates, more mature fine grained clastics, and red-bed formations initially in the north and later throughout the whole suture zone during Eocene to Mid-Oligocene, (3) post-tectonic emplacement of the Zahedan granite during Mid-Oligocene-Miocene. The latter stage is marked also by emplacement of alkaline igneous complexes such as Asagi, Maleksiah-Kuh and Lar igneous suite in the north and central part of the suture zone. The subduction polarity of the Sistan Ocean and its detailed tectonic history is disputed (Arjmandzadeh et al., 2011; Beydokhti et al., 2015). So, the Eocene-Oligocene calc-alkaline magmatism in the Sistan suture zone has been related either to subduction (Richards et al.,

2012), back-arc (Richards, 2015), or post-collisional origin (Ghafaribijar, 2010; Pang et al., 2013).

The Lar Igneous Suite (LIS), with a northwest trend, is located 22 km north of Zahedan in eastern Iran (Fig.1a) and comprises silica-undersaturated to over-saturated intrusive-hypabyssal rock types such as lamprophyres, shonkinite, syenite, nepheline syenite, monzonite, tuffs and breccias. They are exposed as a series of stocks, dykes, sills, volcanic vents, lava flows, and pyroclastics. The LIS syenitic rocks crop out mainly as a giant ring dike and several stocks. The dike is variable in size, width and dip through east to west.

Sample materials and analytical methods

Sampling and optical thin section petrography

Samples were collected from different dikes, stocks and sills during fieldwork for detailed petrographic observations and whole-rock geochemical analyses. Minimum sample size was 1-2 kg (~2 L in volume) to ensure representativity for bulk whole-rock geochemistry, in particular trace elements (see below). Visually altered and/or discolored sample material was as much as possible avoided during field sampling.

Standard size thin sections 27×47 mm of 30 µm nominal thickness were prepared using (bonded diamond discs/silicon carbide slurries) following ABC procedures. Finished sections were polished with 1.0 µm diamond paste on cloth to obtain a mirror shine.

Finalized sections were studied in an Olympus BX51 petrographic microscope in plane and cross-polarized transmitted light. Mineral modal contents in volume percent (vol%) were estimated using the nomograms of Shvetsov in Terry and Chilingar (1955). Suitable spots for *in-situ* assessment of mineral compositions by electron-probe micro-analysis (EPMA; see

below) with perfect surface finish, free from mineral or fluid inclusions, and well-defined mineral grain boundaries were carefully preselected.

Mineral chemistry by EPMA

Prior to analysis, polished sections were covered with 20 nm of carbon in a KLM456 thermal evaporation coating device, to avoid charging in the electron beam.

Electron-probe micro-analyses of olivine, clinopyroxene, mica and feldspar minerals were carried out by using Cameca SX-50 electron microprobe in the Department of Earth, Ocean and Atmospheric Sciences at the University of British Columbia, Canada. The instrument is equipped with four wavelength-dispersive spectrometers (WDS) with a range of LIF, PET and TAP crystals, as well as a Kevex energy-dispersive spectrometer (EDS). The instrument is operated at high vacuum ($<10^{-4}$ mPa), with an acceleration voltage of 15 kV and a beam current of 20 nA (on Faraday cup), and nominal beam diameter of 2-5 μm as observed from the beam imprint.

The EPMA instrument was internally calibrated against mineral standards of natural and synthetic origin, including albite (Na, Al), orthoclase (K), forsterite (Mg), fayalite (Fe), diopside (Ca, Si), chromite (Cr), rutile (Ti), Ni_2SiO_4 (Ni) and rhodonite (Mn). All elements were measured on their respective *K*α lines. SI and Al were measured by EDS, all other elements by WDS, Na at the beginning of each analytical run to minimize migration effects. Spectra were collected with on-peak counting times of 20 seconds, and off-peak upper and lower background for 10 seconds.

Raw element data were ZAF-corrected using the XPP-algorithm of Pouchou and Pichoir (1991) as implemented in the proprietary instrument software. Corrected element contents were converted to stoichiometric oxides in weight percent (wt%); FeO^T represents total iron (oxide) content. The hydrous content of mica as OH was calculated by balance with [F+Cl] to 4.000

apfu, the wt% H_2O was reverse-calculated from that. Unnormalized analytical sum totals (including H_2O-content for micas) are within 100.00±1.50 wt%; values <98.5 wt% or >101.5 wt% are discarded as inferior. Lower limits of detection (LLD) are on the order of 0.10-0.01 wt%, and are specified per element (oxide) in a separate column in the data tables.

Finally, weight percentages oxides of good analytical results were recast into mineral composition formulae in numbers of cations in **a**toms **p**er **f**ormula **u**nit (apfu) following current IMA-approved nomenclature and classification (as applicable), ie. Morimoto et al. (1988) for pyroxenes, Rieder et al. (1998) for micas, Ribbe (1983) for feldspars, and Deer et al. (2013) for olivines.

Bulk whole-rock geochemistry of main and trace elements

Fifteen samples without visible alteration and/or discoloration were selected for whole rock geochemical analysis. Representative rock samples were comminuted in a jaw breaker to pass a 2 mm sieve. The grit was then homogenized and split by cone-and-quartering to obtain a <50 g subsample for pulverization in an agate-lined shatterbox, to pass a 200 mesh (<74 µm) sieve. Powders were collected, homogenized, and stored in screw-capped polyethylene vials. About 5 g of thus powdered sample material was sealed in polyethylene bags for analysis at ALS Chemex Geochemistry Laboratories in Vancouver/CA.

Carefully weighed amounts of 0.100 g of sample powder were turbula-mixed with excess Li-metaborate in 1:4 ratio and digested at ~1 050 °C in a 95Pd05Au crucible. The red-hot melt was poured directly into 125 mL of dilute 0.1 N nitric acid (HNO_3) under constant stirring until completely dissolved, cf. the method of Ingamells (1964). The solution was then made up to 200 mL with 0.1 N nitric acid, ready for assay by inductively-coupled plasma – atomic emission spectroscopy (ICP-AES) for main elements cf. ALS Chemex procedure ME-ICP06, and for inductively-coupled plasma – mass spectrometry (ICP-MS) for trace and rare earth elements

(REE) cf. procedure ME-MS81. Main element concentrations were recalculated into oxides in weight percent (wt%). $Fe_2O_3^T$ represents total iron (oxide) content.

Ignition loss (LOI) was determined gravimetrically on a separate sample aliquot. A carefully weighed 5.000 g amount of sample powder was predried at 105 °C, then ignited at ~1050 °C in a graphite crucible for 2h, and the weight difference recorded as LOI in wt%.

Blanks, blind duplicates and accredited and in-house standards were interspersed throughout the sample series for quality control purposes. For bulk whole-rock analysis of main element oxides including ignition loss LOI, analytical sum totals are within 100.00±1.50 wt%; results outside that range were disregarded. Lower limits of detection (LLD) are specified per element (oxide) species in a separate column in the data tables.

Results

Petrography

The rocks in the LIS are syenite to alkali-feldspar syenite in composition. They show porphyritic texture with megacrysts and phenocrysts of K-feldspar (orthoclase and microcline, 55-75 vol%), plagioclase (10-17 vol%, An_{5-47}), biotite (12-20 vol%), clinopyroxene (5-10 vol%) and olivine (<5 vol%) which are set in a medium to fine grained groundmass of all aforementioned minerals. Quartz is rare or completely absent. Apatite and titanite are the most common accessory minerals. K-feldspars are often crowded mainly by microphenocrysts of plagioclase and biotite which have been arranged in parallel orientation along the crystallographic surface of the host megacrystes (Fig.2a); in addition, they show exsolution textures in the form of microperthite and patch perthite. Plagioclase phenocrysts demonstrate k-feldspar overgrowth as anti-rapakivi texture (Fig.2b). Most biotite lathes exhibit strong

absorbed margins and kink-band microtexture (Fig.2b). Clinopyroxene grains are mostly colorless to pale green; in some cases they show optical zoning, absorbed margins and sieve micro texture. Olivines are altered to iddingsite and other subsolidus re-equilibration reactions in the form of opaque minerals.

Mineral chemistry

Olivine

Olivine exhibits a relatively narrow range of forsterite component ($Fo_{78–80}$ mol %) (Table 1). The concentration of CaO in the study olivines is relatively low (0.06-0.14 wt%), but a slightly higher than those crystallized from primitive mantle-derived magmas (CaO< 0.1 wt%; Foley et al., 2011). The NiO content is often very low (0.04-0.14 wt%) which implies the olivine is not mantle derived (Ni<2500 ppm; Foley et al., 2011) (Fig. 3); which seems confirmed by the high MnO concentrations (0.77-1.14 wt%) that are higher than those from mantle-derived olivines (MnO= 0.09-0.17; Foley et al., 2011). The high Mn levels and consequently high Mn/Fe ratios has been related either to fractionation (Foley et al., 2013) or carbonatite metasomatism (Ammanati et al., 2016).

Clinopyroxene

Table 2 shows representative compositions of clinopyroxenes in the LIS syenites. Most clinopyroxenes plot in the salite field, and some in the augite field in wollastonite-enstatite-ferrosilite ternary diagram. Almost all phenocrysts show normal compositional zoning, based on decreasing MgO content from core to rim. They are also characterized by low content of TiO_2 (0.24-1.24 wt%) but high CaO (20.42-22.95 wt%) and Na_2O (0.61-1.30 wt%). The high

Al_2O_3 content in the study clinopyroxenes correlates well with that of the bulk rock composition; in the other hand, the Al_2O_3 content is higher than values in diopside (Al_2O_3 < 2 wt%; Knittel and Cundari, 1990) and also higher than those reported from clinopyroxenes in peralkaline magmas (Al_2O_3 < 0.5 wt%; Eriksson, 1982). The high Al content has also led to these clinopyroxenes being classified within the field of Roman-type potassic rocks that confirms their relation to an orogenic system (Fig. 4). In addition, the high Al/Ti ratio (4.37-17.14) has been attributed to low pressure fractionation (Tappe et al., 2006).

Mica

Representative chemical analyses of micas are given in Table 3. The micas in the LIS syenites have high MgO (12.29–19.08 wt%) and Mg# (55.3-79.7) and most classified as magnesian biotites (Fig. 5a). The concentration of TiO_2 (2.91-5.54 wt%) and Al_2O_3 (13.75–15.35 wt%) is relatively low. Their FeO content is also variable (8.69-18.32 wt%) and as a result the 100*Fe/(Fe^{2+}+Mg) ratio varied from 20.3 to 44.5. The large rang of Mg# and Fe/(Fe^{2+}+Mg) ratio demonstrates mineral evolution during magma fractionation. The FeO/MgO ratio in the studied biotites varied from 0.46 to 1.44 that is lower than host syenites (1.32-6.35), suggesting more evolved magma and less equilibrated biotites with the host magma; the data imply that the most biotites in the LIS syenites are primary and less re-equilibrated (Fig. 5b).

Feldspars

The K-feldspars are the most abundant feldspar in the LIS syenites. Their chemical compositions are in the range $Or_{52.6}$ $Ab_{45.1}$ $An_{2.3}$ to $Or_{84.3}$ $Ab_{15.3}$ $An_{0.4}$ indicating their potassium rich composition (Table 4). The K-feldspars are characterized by low CaO content (0.09-0.81 wt%). They have fairly high abundances of Na_2O (1.72-5.61 wt%) and low Fe_2O_3 content (0.08-

0.39 wt%) which is typical of K-feldspars from Roman-type rocks (Conticelli, 1998; Mitchell and Bergman, 1991). In the other hand, chemical composition of plagioclase is variable, ranging between Ab_{53} (andesine) and Ab_{95} (albite) which implies continues change in the mineral composition during magma evolution.

Bulk whole-rock main and trace elements

The chemical composition of LIS syenitic rocks is given in the Table 5. Most samples have high Sr/Y (>27) and La/Yb (>20) ratios that is typical of adakitic rocks (Defant and Drummond, 1990). They also display large range of SiO_2 (54.0-68.3 wt%), MgO (0.34-4.72 wt%) and Mg# (23.7-57.7), as well as relatively high Al_2O_3 (15.7-19.1 wt%) contents. In addition, the TiO_2 content in the LIS syenites is relatively low (0.20-0.82 wt%). All samples in the TAS diagram display alkaline affinities and plot in the syenite, foid syenite and foid monzosyenite fields. Compared to typical adakites (Kay, 1978; Yogodzinski et al., 1995), the LIS syenitic rocks relevant to shoshonitic series with high K_2O contents (4.82-7.87 wt%) and K_2O/Na_2O ratios ranging from 0.86 to 1.99.

The LIS syenites are characterized by high LREE and relatively low HREE concentrations, along with a clear LREE/HREE fractionation (e.g. La/Yb= 7.5–29.3). The rocks also display strongly fractionated MREEs that resulting a low $(Gd/Yb)_N$ = (0.9-2.4) ratios and nearly flat HREE and MREE patterns (Fig. 6a). In addition, they show a negative Eu anomalies (Eu/Eu* = 0.25-0.95).

They are also enriched in LILEs (i.e., Rb, Sr, Th and U). Their primitive mantle normalized incompatible trace element patterns (Fig. 6b) are characterized by negative Nb, Ta, Ti and Ba anomalies that is typical of orogenic magmas (Drummond and Defant, 1990; Rudnick, 1995; Taylor and McLennan, 1995; Gao et al., 2010). Negative Ba anomalies are also reported in high-K and Roman Province shoshonitic rocks (Conticelli et al., 2007). Almost all

samples have high and variable Sr contents (88–1135 ppm); the high Sr anomalies and low Nb, Ta and Ti (Fig. 6b) are typical features of adakitic magmas (Martin et al., 2005).

Discussion

Fractional crystallization

The major and trace elements reported in Table 5 clearly show the important role of fractional crystallization in the study rocks. Fractional crystallization is considered as a way to generate syenitic magmas (Parker, 1983; Brotzu et al., 2007). In the other hand, the adakitic features (i.e. high Sr/Y and La/Yb ratios) are also achieved by hydrous (involving amphibole) or high-pressure (involving garnet) crystal fractionation of a mafic magma (Richards and Kerrich, 2007; Moyen, 2009). The decrease in $Fe_2O_{3(t)}$, MgO, CaO and TiO_2 content (Fig. 7a, b, d and e) indicate a fractional crystallization of ferromagnesian minerals such as olivine, clinopyroxene and biotite. The compatible trace elements (e.g., Ni and Cr) in the LIS syenites show similar trends to $Fe_2O_{3(t)}$ and MgO that emphasis fractional crystallization of ferromagnesian phenocrysts. Interestingly, the Al_2O_3 display an opposite trend to K_2O at approximately 59 wt% of SiO_2 (Fig. 7c and g); this confirms the onset of K-feldspar fractionation when the SiO_2 content in the magma reaches to 59 wt%. However, the Na_2O content in the LIS syenites continuously increases (Fig. 7f), suggesting onset of plagioclase crystallization in the late stages of magmatic evolution. The CaO/Al_2O_3 ratio is sensitive to plagioclase and clinopyroxene fractionation; the ratio increases with fractionation of plagioclase and decreases with clinopyroxene fractionation, respectively (Ferreira and Murton, 2014). The CaO/Al_2O_3 ratio in the LIS syenites decreases during magma evolution (Fig. 7h); this enforces that clinopyroxene has controlled the CaO content in the magma.

Feldspar fractionation is supported by significant depletions in Ba and Eu in the primitive mantle-normalized multi element diagram (Fig. 6b); the concentration of Ba in the study rocks also demonstrates positive correlation with Eu/Eu^{*} ratios; this indicates that alkali feldspars have been removed during magma evolution. In the other hand, the most negative Eu anomalies can be seen in the most evolved samples, which suggests that the fractionation of plagioclase at the late stages of magma evolution has intensified the negative Eu anomalies. We concluded that the increase in the Rb/Sr ratio with the decrease in Sr content and positive correlations between Ba and Sr contents are the results of alkali feldspar and plagioclase, along with biotite fractionation.

The LIS adakitic syenites are characterized by high K_2O and K_2O/Na_2O ratios; these features cannot be considered as a result of magmatic differentiation, because the K_2O/Na_2O ratio has negative correlation with the SiO_2 content (Fig. 8a). Moreover, crystal fractionation of a mafic magma results in a high La/Yb ratios in more evolved magmas (Castillo et al., 1999; Macpherson et al., 2006), while in the LIS syenites this ratio systematically decreases with increasing SiO_2 content (Fig. 8b). In addition, a fractional crystallization model to produce syenites with adakitic signatures requires the occurrence of an extremely large amount of parental magma bodies, such as andesitic and basaltic magmatism; the evidence for which is lacking in the study area. Therefore, we suggest that although fractional crystallization must have occurred during syenite formation, this cannot be considered alone for the high K_2O content and adakitic signatures.

Crustal contamination

Crustal contamination has important role in the modification of any magma (DePaolo, 1981; Thompson et al., 1982; Dostal and Dupuy, 1984). It can be evaluated by isotopic data and also by the trace element geochemistry. Scarrow et al., (2009) believe that crustal contamination in

potassic rocks will be better reflected in trace element geochemistry. They believe that melts derived from metasomatised mantle with slightly crustal contamination are characterized by low Cs (<5 ppm) and high Rb/Cs ratio (>40). The LIS syenites have high Cs (4.35-21.50 ppm; except for sample 12 with Cs=0.82 ppm) and relatively low Rb/Cs ratios (12.8-59.7; with the exception of sample12 with Rb/Cs=181.1). Zhang et al., (2008) pointed out that low Th/Ce ratios and absence of negative Eu anomalies suggest that crustal contamination does not play a significant role in the modification of magmas because continental crust has relatively high Th/Ce ratios (~ 0.15) and negative Eu anomalies (Taylor and McLennan, 1995), in contrast to mantle-derived magmas that have low Th/Ce ratios (0.02-0.05, Sun and McDonough, 1989). Negative Eu anomalies as well as relatively high Th/Ce ratios (0.15-0.90) in the LIS syenites confirm that crustal contamination is a major process in the magma modification. Although negative Nb and Ta anomalies are attributed to arc magmas, crustal contamination can also cause their depletion in magma (Guo et al., 2004). The enrichment of Th and U relative to La in the LIS syenitic rocks (Fig. 6b) supports the possibility of significant upper–middle crustal contamination (Taylor and McLennan, 1985). Whereas contamination by lower crustal rocks with relatively low Sr abundance (e.g., 350 ppm, Rudnick and Fountain, 1995) can cause a Sr decrease in the melts. This is in contrast to magma differentiation trend, in which the Sr content moderately increases in the magma. Although the Sr content in the LIS syenites decreases with increasing SiO_2, but its content is much higher than that of lower crust; therefore, it is unlikely that the lower crustal contamination has been involved in the magma evolution of the studied samples. So, upper-middle crustal contamination on the magma evolution may have played a major role in the genesis of LIS syenites.

Petrogenesis

In the LIS syenites the K_2O/Na_2O and La/Yb ratios decrease with increasing SiO_2 content (Fig. 8a, b); this pointed out that fractional crystallization cannot cause potassic and adakitic features in the LIS syenitic rocks. In addition, the positive correlations of La/Yb and La/Sm ratios with La content confirm that partial melting, rather than fractionation, has more important role in the whole rock geochemical variations (Fig. 8c, d). Crustal rocks as a possible source, can be ruled out because experiments show that partial melting of any crustal rocks and even lower crustal intermediate-mafic rocks in the deep crust would produce high-Si, low-Mg liquids(e.g., Yang et al., 1993; Zhang et al., 1994; Gao et al., 1998; Rapp et al., 2003); partial melting of a mafic lower continental crust generates magmas with Mg# lower than 45 (Wang et al., 2007), or even lower than 40 (Rapp and Watson, 1995). While the syenitic rocks in the study area are intermediate in composition with Mg# range between 23 and 58.

The high and variable silica content (54.0-68.3 wt.%), high K_2O and K_2O/Na_2O ratio and relatively low concentration of Cr (10-150 ppm) and Ni (13-78 ppm) suggest that the derivation of the LIS syenitic magma directly from a mantle source, without considering other means such as fractional crystallization and crustal contamination, must be unlikely. However, it has been generally accepted that the majority of potassic rocks are derived by partial melting of a continental lithospheric mantle modified by subduction related fluids and/or melts (Jiang et al., 2002; Rogers et al., 1998). The depletion in HFSEs is usually considered as an indication of subduction processes in the mantle source (Sun and Kerrich, 1995). Gill (1981) pointed out that high Ba/Nb (>28) ratio is the most significant geochemical characteristic of island-arc magmas with an enriched mantle source. In the plot of Ba/Zr vs. Nb/Zr ratios, it is apparent that almost all LIS syenites have been derived from an enriched lithospheric mantle source with high Ba/Nb ratios (Fig. 9b). In geochemical discrimination diagrams such as Al_2O_3 vs. TiO_2 and Zr (ppm) vs. Y (ppm) the LIS syenites clearly show subduction related potassic affinities. Falloon et al., (1988) experimentally confirmed that depleted peridotite is characterized by low total Fe_2O_3 (<10 wt%) and low TiO_2 (<2 wt%). In the plot of TiO_2 vs. Fe_2O_3 the LIS syenites fall within

and close to the field of depleted peridotite (Fig. 9a); it shows that the lithospheric mantle source of the study rocks must have been a depleted source before being affected by enrichment processes.

The depletion of HFSEs in the study rocks indicates that the asthenosphere metasomatic melts are unlikely to have been contributed in the mantle (Hofmann, 2003). Moreover, the Nb/U ratio (2.06–3.94) in the LIS syenites is significantly lower than those in mid ocean ridge basalts and ocean island basalts (Nb/U=47; Hofmann, 2003), and even lower than lower continental crust (Nb/U=25; Rudnick and Gao, 2003), but is close to estimated average composition of globally subducted sediments (Nb/U= 5; Plank and Langmuir, 1998); this suggests that the lithospheric mantle source has been metasomatized most probably by fluids and/or melts with a composition similar to upper continental crust. In the other hand, one of the most important signatures of clay, chert and carbonated ooze is their negative Ce anomalies (Taylor and McLennan, 1995); the Ce/Ce* ratios in almost all LIS syenites is lower than 1. Schreiber et al (1980) pointed out that none of igneous processes can cause negative Ce anomalies in the magma. Therefore, the negative Ce anomalies in arc related magmas shows the involvement of oceanic sediments, also as a source for potassium, in the mantle source region. So, upper crustal contamination can be considered in the upper mantle source through subduction process. Li et al., (2014) believe that these geochemical signatures, along with low TiO_2 content, strong fractionation between LREE and HREE, enrichment of LILE and depletion of HFSE indicate that the parental magma most probably have originated from a lithospheric mantle source enriched by subducted components.

Origin of high Sr/Y and La/Yb

The term adakite was initially defined by Defant and Drummond (1990) for rocks derived from melting of young subducted oceanic crust. Adakites have distinctive geochemical signatures

such as SiO_2 ≥56 wt%, Al_2O_3 ≥15 wt%, K_2O/Na_2O ~ 0.4, high La/Yb and Sr/Y ratios (see e.g., Defant and Drummond, 1990; Richards and Kerrich, 2007). In geochemical discrimination diagrams such as La/Yb vs. La (Defant and Drummond, 1990), almost all studied samples plot in the field of adakites (Fig. 10a). Noteworthy, in contrast to typical slab-derived adakites that are characteristically sodium-rich (Liu et al., 2010; Richards and Kerrich, 2007), the LIS adakitic syenites are potassium-rich (K_2O/Na_2O = 0.86–1.99). Their high K_2O contents and high K_2O/Na_2O ratios are considered as a distinctive feature of continental adakites (potassic adakites; Moyen, 2009). Ghafaribijar (2010) established that the Oligocene K-rich magmatism in the LIS has been occurred in a post-collisional arc setting. Recent studies revealed that, beside partial melting of a young subducted oceanic crust, there are several other mechanisms for the generation of adakitic rocks; such as partial melting of a foundering (delaminated) lower continental crust (Gao et al., 2004; Wang et al., 2007), melting of a thickened mafic lower-crust (Atherton and Petford, 1993; Hou et al., 2004), and magma assimilation and fractional crystallization (AFC) of basaltic melts (Castillo et al., 1999; Macpherson et al., 2006).

The lack of a large volume of coeval mafic rocks rules out high or low pressure fractional crystallization of basaltic melts as a possible way to generate syenites with adakitic signatures (Chung et al., 2005). Partial melting, in contrast to fractional crystallization, plays an important role in the geochemical characteristics of LIS syenites (Fig. 8c, d). Partial melting of a thickened mafic lower crust is able to produce adakitic magmas with high K_2O contents and K_2O/Na_2O ratios (Castillo, 2006; Liu et al., 2010); It has been argued that partial melting of a mafic Lower continental crust under high pressure at the presence of garnet can produce magmas with high K_2O contents and high K_2O/Na_2O ratios (Liu et al., 2010). However, the REE enrichment in the LIS syenites (Fig. 6a), with $(La/Yb)_N$=12.3–19.6 and $(Gd/Yb)_N$=0.9–2.4, suggests that their parental magmas have been generated at depths where spinel is a residual phase (Ellam, 1992). Note withstanding, the variable range of Mg# (23-58) in the LIS syenites rules out this mechanism; because Mg# in some samples is higher than expected values for magmas produced

by partial melting of lower continental crust (Mg# <45 or <40). They have also a restricted Th/U ratio (3.02–3.75), which is significantly lower than the lower crust-derived melts (Th/U = 3-50; Ling et al., 2011). Moreover, although Sr content decreases with increasing SiO_2 content in the LIS syenites, their initial values, in less evolved samples, are much higher than those expected from melting of lower mafic continental crust (e.g., 350 ppm, Rudnick and Fountain, 1995).

Due to variable Mg#, Cr and Ni content, partial melting of a delaminated lower crust is another way that can be considered for the generation of LIS syenites; in most cases, melts derived from a foundered or delaminated thickened lower crust would also interact with the overlying mantle peridotite during magma ascent, resulting in elevation of the Mg#, Cr and Ni in the adakitic magmas (Castillo, 2006; Wang et al., 2007). Although, the amount of Mg#, Cr and Ni in the LIS syenites is variable, but is higher than adakitic rocks derived by partial melting of delaminated thickened lower crust worldwide (Fig. 12a, b). Noteworthy, almost all clinopyroxene grains in the LIS syenites show normal compositional zoning; normal zoning rules out the hypothesis of magma mixing between delaminated lower crust-derived magmas and more primary mantle-derived melts (Shao and Lu, 2008)

The other alternative model for the adakitic signatures in LIS syenites is partial melting of a subducted oceanic slab. The high Sr/Y and La/Yb ratios and positive Sr anomalies in the LIS syenites, although, points to slab-derived melts, but they are K-rich which is inconsistent with Na-rich slab-derived adakites. In addition, there is no positive correlation between La/Yb and Sr/Y ratios (Fig. 10b), suggesting a decoupling of Sr/Y and La/Yb ratios which comparable to arc adakites from modern subduction zones (Liu et al., 2010; Ling et al., 2011). Meanwhile, restricted range of Th/U ratios (3.02–3.75) is similar to melts derived from oceanic crust (Th/U ~ 3; Ling et al., 2011). In the plot of Cr and Ni vs SiO_2 content, the LIS syenites have higher and more variable Cr and Ni content compared to adakites derived by partial melting of delaminated lower crust and also thickened lower crust, but show relatively similar trends to

subducted oceanic crust derived adakites (Fig. 12a, b). Gao et al., (2010) believe that the positive correlation between Sr/Nb and Gd/Yb ratios along with negative correlation between Rb/Sr and Sr/Y ratios confirm the presence of slab components of basaltic oceanic crust and subducted sediment melts in the mantle source, respectively (Fig. 11a, b). So, it seems that the mantle source of the studied samples have been experienced sediment and basaltic oceanic slab melts as major metasomatic agents in the mantle source.

The Oligocene LIS syenites are the result of post-collision magmatism in the Sistan suture zone. The theory that slab melts may have been a common occurrence in continental settings is hard to accept. A direct partial melting of young and hot slabs seems unlikely to have led to the generation of the post-collision adakitic magmas in the LIS; slab melts may possibly be involved in the arc magma genesis without being necessarily emplaced at the surface (Maury et al., 1992; Kelemen et al., 2003). Richards and Kerrich (2007) believe that pure slab melts are probably never erupted at the Earth surface; but instead they are considered as an effective metasomatic agent which have interacted and probably frozen in the mantle. Partial melting of such metasomatized mantle source would produce magmas which are a mixture of primary felsic slab melts and the actually more mafic depleted mantle peridotite components. Geochemical data point out that sub continental lithospheric mantle in the Lar region has been modified by melts released from subducted oceanic slab including basaltic oceanic crust and subducted sediments.

Origin of potassium

In previous sections it was confirmed that the unusual K_2O enrichment in the LIS syenites has not been simply a result of magmatic differentiation, but is a primary feature which can be related to the geochemical signatures in the source region. There are two possibility for the origins of relatively high K_2O contents in the LIS adakitic syenites: (i) a source with high K_2O

contents such as metasomatized mantle (Rapp *et al*., 2002), (ii) the source rocks with low K_2O contents, but the magma were generated by low degree partial melting of lower continental crust at high pressures, resulting in relatively high K_2O content (Rapp *et al*., 2002; Huang and He, 2010).

As discussed in previous sections, potassium-rich and adakitic nature in the study rocks are not related to partial melting of thickened mafic lower continental crust at high pressure. So, the high K_2O content in the LIS adakitic syenites has been probably inherited from a source region with high K_2O contents. Rogers et al. (1987) invoked sediment subduction for the genesis of potassium in orogenic lavas that typically have high Rb/Sr and Rb/Ba ratios (Fig. 12c). A silicate melt derived from partial melting of subducted pelitic sediments would contain significant K_2O (Woodard et al., 2014); it can infiltrates into the mantle wedge, likely as veins. The high abundances of K_2O (4.82–7.87 wt%) and the lack of its correlation with SiO_2 indicates variable degrees of partial melting at the presence of a potassic phase in the mantle source region (e.g., phlogopite or amphibole; Stolz et al., 1996). Phlogopite can provide higher contributions of Ba and Rb, but less Sr, than amphibole (Foley et al., 1996; Furman and Graham, 1999). Noteworthy, the partition coefficient for Ba is higher than Rb in phlogopite and is reverse in amphibole (Foley et al., 1996). Consequently, partial melting of a phlogopite-bearing mantle source are expected to produce melts with significantly higher Rb/Sr (>0.1) and lower Ba/Rb (<20) ratios compared to melts formed by partial melting of an amphibole-bearing mantle source (Furman and Graham, 1999). The LIS syenites have high Rb/Sr and low Ba/Rb ratios, strongly suggest that these rocks were all derived from melting of a phlogopite-bearing source (Fig. 12d).

Conclusion

516 The Oligocene Lar igneous suite (LIS) in the central part of the Sistan suture zone, comprises
517 a variety of silica under saturated to slightly silica over saturated intrusive, hypabyssal and
518 extrusive rock types such as lamprophyres, shonkinite, syenite, nepheline syenite, monzonite,
519 tuff and breccia. The syenites crop out mainly as a giant ring dike and several related stocks.
520 Their composition varies from syenite to alkali-feldspar syenite, containing megacrystes and
521 phenocrysts of K-feldspars (Or_{52-84}, Ab_{15-45}, $An_{0.4-2.0}$), plagioclase (Ab_{53-95}), biotite (Mg# 53-
522 79), pyroxene ($Wo_{43.3-48.0}$, $En_{35.0-44.9}$, $Fs_{9.9-16.9}$) and olivine (Fo_{78-80}) set in a groundmass of all
523 aforementioned minerals. High abundance of Al_2O_3 in clinopyroxenes and high Na_2O and low
524 Fe_2O_3 contents in K-feldspars are typical of orogenic systems.

525 The LIS adakitic syenites, in comparison to typical adakites, are shoshonitic in
526 composition. They have variable SiO_2 and MgO, as well as relatively high Al_2O_3 but low TiO_2
527 content. They are also characterized by enrichment in LILE and LREE, fractionated
528 LREE/HREE and MREE/HREE, depleted in HFSEs and high Sr/Y and La/Yb ratios. Negative
529 Ba, Nb, Ta, Ti and positive Th, U anomalies point out to their orogenic nature. Geochemical
530 data define the lithospheric mantle-derived magmas, as the origin of LIS syenites, which have
531 experienced fractionation and minor contamination by middle-upper crustal materials. It is
532 apparent that partial melting events, rather than fractionation, have a more important role in the
533 geochemical variations. Although some fractional crystallization must have been occurred
534 during the formation of the LIS syenites but it cannot alone account for the high K_2O content
535 and adakitic signatures. High K_2O content in the LIS syenites is not simply as the result of
536 magmatic differentiation but is a primary feature that is related to the geochemical signatures
537 in the source region; high Rb/Sr (>0.1) and low Ba/Rb (<20) ratios confirm the residual
538 phlogopite as the most important K-bearing phase in their mantle source region. We believe
539 that the LIS post-collisional adakitic syenites have originated by partial melting of SCLM
540 source metasomatized by hybrid subducted oceanic slab-derived adakitic melts and sediment
541 melts. The slab metasomatic events in the Sistan mantle wedge have taken place during the

closure of the Sistan Ocean, one of the branches of Neotethys Ocean. Subsequent partial melting in a post-collision setting likely associated with decompression, gave rise to syenitic magmas.

Acknowledgments

This article was extracted from the PhD thesis by Sasan Ghafaribijar at Shahid Bahonar University of Kerman. The first author also expresses his appreciation to the National Iranian Copper Industries Company (NICICO) for providing the facilities required to carry out the field work at the Lar area. We also acknowledge an anonymous reviewer for his/her comments that helped improve the manuscript.

Declaration of interests

☒ The authors declare that they have no known competing financial interests or personal relationships that could have appeared to influence the work reported in this paper.

☐The authors declare the following financial interests/personal relationships which may be considered as potential competing interests:

References

Agard P, Omrani J, Jolivet L, Whitechurch H, Vrielynck B, Spakman W, Monié P, Meyer B, Wortel R (2011). Zagros orogeny: a subduction-dominated process. Geol Mag 148: 692–725.

Alavi M, Vaziri H, Seyed-Emami K, Lasemi Y (1997). The Triassic and associated rocks of the Nakhlak and Aghdarband areas in central and northeastern Iran as remnants of the southern Turanian active continental margin. Geol Soc Am Bull 109: 1563–1575.

Ammannati E, Jacob DE, Avanzinelli R, Foley SF, Conticelli S (2016). Low Ni olivine in silica-undersaturated ultrapotassic igneous rocks as evidence for carbonate metasomatism in the mantle. Earth Planet Sci Lett 444: 64–74.

Arjmandzadeh R, Karimpour MH, Mazaheri SA, Santos JF, Medina JM, Homam SM (2011). Two-sided asymmetric subduction; implications for tectonomagmatic and metallogenic evolution of the Lut Block, eastern Iran. J Econ Geol 3 (1): 1–14.

Atherton MP, Petford N (1993). Generation of sodium-rich magmas from newly underplated basaltic crust. Nature 362, 144–146.

Beydokhti RM, Karimpour MH, Mazaheri SA, Santos JF, Klötzli U (2015). U–Pb zircon geochronology, Sr–Nd geochemistry petrogenesis and tectonic setting of Mahoor granitoid rocks (Lut Block, Eastern Iran). J Asian Earth Sci 111: 192–205.

Brotzu P, Melluso L, Bennio L, Gomes CB, Lustrino M, Morbidelli L, Morra V, Ruberti E, Tassinari C, D'Antonio M (2007). Petrogenesis of the Early Cenozoic potassic alkaline complex of Morro de São João, southeastern Brazil. J South Am Earth Sci 24: 93-115.

Castillo PR (2006). An overview of adakite petrogenesis. Chinese Sci Bull 51: 258–268.

Castillo PR, Janney PE, Solidum RU (1999). Petrology and geochemistry of Camiguin Island, southern Philippines: insights to the source of adakites and other lavas in a complex arc setting. Contrto Mineral Petrol 134: 33–51.

Chaffey DJ, Cliff RA, Wilson BM (1989). Characterization of the St. Helena magma source. In: Saunders AD, Norry MJ (eds) Magmatism in the ocean basins. Geol Soc London, Spec Publ 42: 257–276.

Chance P (1981). Petrogenesis of a low- Ti, potassic Suite: Kuh-e Lar caldera subsidence complex, eastern Iran. Unpublished MSc Thesis, University of Western Ontario (London) 166pp.

Chung SL, Chu MF, Zhang Y, Xie Y, Lo CH, Lee HY, Lan CY, Li X, Zhang Q, Wang Y (2005). Tibetan tectonic evolution inferred from spatial and temporal variations in post-collisional magmatism. Earth Sci Rev 68: 173–196.

Conticelli S, Francalanci L, Manetti P, Cioni R, Sbrana A (1997). Petrology and geochemistry of the ultrapotassic rocks from the Sabatini Volcanic District, Central Italy: the role of evolutionary processes in the genesis of variably enriched alkaline magmas. J Volc Geotherm Res 75: 107–136.

Conticelli S, Carlson RW, Widow E, Serri G (2007). Chemical and isotopic composition (Os, Pb, Nd, and Sr) of Neogene to Quaternary calc-alkaline, shoshonitic, and ultrapotassic mafic rocks from the Italian peninsula: Inferences on the nature of their mantle sources. In: Beccaluva L, Bianchini G, Wilson M (eds): Cenozoic volcanism in the Mediterranean Area. Geol Soc Am, Spec Pap 418: 171–202.

Deer WA, Howie RA, Zussman J (2013). An introduction to the rock forming minerals. 3rd Edition. Geol Soc London, London/UK, pp549

Defant MJ, Drummond MS (1990). Derivation of some modern arc magmas by melting of young subducted lithosphere. Nature 347: 662–665.

Defant MJ, Kepezhinskas P, (2001). Evidence suggests slab melting in arc magmas. Eos, Transact Am Geophys Union 82: 65–69.

DePaolo DJ (1981). Trace element and isotopic effects of combined wall rock assimilation and fractional crystallization. Earth Planet Sci Lett 53: 189-202.

620 Dostal JB, Dupuy C (1984). Geochemistry of the North Mountain Basalts (Nova Scotia,
621 Canada). Chem Geol 45: 245-261.
622 Drummond MS, Defant MJ (1990). A model for trondhjemite–tonalite–dacite genesis and
623 crustal growth via slab melting: Archean to modern comparisons. J Geophys Res 95:
624 21503–21521.
625 Ellam RM (1992). Lithospheric thickness as a control on basalt geochemistry. Geol 20: 153–
626 156.
627 Eriksson SC (1982). Aspects of the petrochemistry of the Phalaborwa Complex, southeastern
628 Transvaal, South Africa. Unpublished PhD Thesis, University of the Witwatersrand,
629 Johannesburg South Africa. 265pp.
630 Falloon TJ, Green DH, Hatton CJ, Harris KL (1988). Anhydrous partial melting of a fertile and
631 depleted peridotite from 2 to 30 kbar and application to basalt petrogenesis. J Petrol 29:
632 1257–1282.
633 Ferreira P, Murton B, (2014). Magmatic differentiation of the least incompatible element
634 enriched lavas from PO-1 segment, 37ºN on the Mid-Atlantic Ridge (MAR).
635 Comunicações Geológicas 101: 105–109.
636 Foley SF, Jackson SE, Fryer BJ, Greenouch JD, Jenner GA (1996). Trace element partition
637 coefficients for clinopyroxene and phlogopite in an alkaline lamprophyre from
638 Newfoundland by LAM-ICP-MS. Geochim Cosmochim Acta 60: 629–638.
639 Foley SF, Jacob DE, O'Neill StC (2011). Trace element variations in olivine phenocrysts from
640 Ugandan potassic rocks as clues to the chemical characteristics of parental magmas. Contr
641 Mineral Petrol 162: 1–20.
642 Foley SF, Prelevic D, Rehfeldt T, Jacob DE (2013). Minor and trace elements in olivines as
643 probes into early igneous and mantle melting processes. Earth Planet Sci Lett 363: 181–
644 191.

645 Foley SF, Venturelli G, Green DH, Toscani L (1987). The ultrapotassic rocks: characteristics,
646 classification, and constraints for petrogenetic models. Earth Sci Rev 24: 81–134.
647 Furman T, Graham D (1999). Erosion of lithospheric mantle beneath the East African Rift
648 system: geochemical evidence from the Kivu volcanic province. Lithos 48: 237–262.
649 Gao S, Luo TC, Zhang BR, Zhang HF, Han YW, Zhao ZD, Hu YK (1998). Chemical
650 composition of the continental crust as revealed by studies in East China. Geochim
651 Cosmochim Acta 62: 1959– 1975.
652 Gao S, Rudnick RL, Yuan HL, Liu XM, Liu YS, Xu WL, Ling WL, Ayers J, Wang XC, Wang
653 QH (2004). Recycling lower continental crust in the North China Craton. Nature 432:
654 892–897.
655 Gao Y, Yang Z, Santosh M, Hou Z, Wei R, Tian S (2010). Adakitic rocks from slab melt-
656 modified mantle sources in the continental collision zone of southern Tibet. Lithos 119:
657 651–663.
658 Ghafaribijar S (2010). Geochemistry of potassic mafic rocks in the Lar Complex, North of
659 Zahedan, East of Iran, Unpublished MSc Thesis, Sistan and Baluchestan University.
660 159pp.
661 Gibson SA, Thompson RN, Leat PT, Morrison MA, Hendry GL, Dickin AP, Mitchell JG
662 (1993). Ultrapotassic magmas along the flanks of the Oligo-Miocene Rio Grande Rift,
663 USA: monitors of the zone of lithospheric mantle extension and thinning beneath a
664 continental rift. J Petrol 34: 187–228.
665 Gill JB (1981). Orogenic Andesites and Plate Tectonics. Springer, Berlin, 390 pp.
666 Guo F, Fan WM, Wang YJ, Zhang M (2004). Origin of early Cretaceous calc-alkaline
667 lamprophyres from the Sulu orogen in eastern China: implications for enrichment
668 processes beneath continental collisional belt. Lithos 78: 291–305.
669 Hofmann AW (2003). Sampling mantle heterogeneity through oceanic basalts: Isotopes and
670 trace elements. Treat Geochem 2: 61–101.

671 Hooper RJ, Baron I, Hatcher RD, Agah S (1994). The development of the southern Tethyan
672 margin in Iran after the break-up of Gondwana — implications for the Zagros
673 hydrocarbon province. Geoscience (Geological Survey of Iran) 4: 72–85.
674 Horton BK, Hassanzadeh J, Stockli DF, Axen GJ, Gillis RJ, Guest B, Amini A, Fakhari MD,
675 Zamanzadeh SM, Grove M (2008). Detrital zircon provenance of Neoproterozoic to
676 Cenozoic deposits in Iran: implications for chronostratigraphy and collisional tectonics.
677 Tectonophys 451: 97–122.
678 Hou ZQ, Gao YF, Qu XM, Rui ZY, Mo XX, (2004). Origin of adakitic intrusives generated
679 during mid-Miocene east–west extension in southern Tibet. Earth Planet Sci Lett 220:
680 139–155.
681 Huang F, He Y (2010). Partial melting of the dry mafic continental crust: Implications for
682 petrogenesis of C-type adakites: Chinese Sci Bull 55: 2428–2439.
683 Irvine TN, Baragar WRA (1971). A guide to the chemical classification of the common volcanic
684 rocks. Can J Earth Sci 8: 523–548.
685 Jiang YH, Jiang SY, Ling HF, Zhou XR, Rui XJ, Yang WZ (2002). Petrology and geochemistry
686 of shoshonitic plutons from the western Kunlun orogenic belt, Xinjiang, northwestern
687 China: implications for granitoid geneses. Lithos 63: 165–187.
688 Kay RW (1978). Aleutian magnesian andesites: melts from subducted Pacific ocean crust. J
689 Volc Geotherm Res 4: 117–132.
690 Kelemen PB, Yogodzinski GM, Scholl DW (2003). Along-strike variation in the Aleutian
691 island arc: genesis of high Mg# andesite and implications for continental crust. In: Eiler
692 J (edr), The Subduction Factory. Am Geophys Union, Monogr 138:223–246.
693 Knittle U, Cundari A (1990). Mineralogical evidence for the derivation of Metaluminous,
694 potassic rocks from peralkaline precursors: The Cordon Syenite Complex (Philippines).
695 Mineral Petrol 41: 163-183.

696 Le Maitre RW, Streckeisen A, Zanettin B, Le Bas MJ, Bonin P, Bateman P, Bellieni G, Dudek
697 A, Efremova S, Keller J, Lameyre J, Sabine PA, Schmid R, Sørensen H, Woolley AR
698 (2002) Igneous rocks: a classification of and glossary of terms. Recomm Int Union Geol
699 Sci (IUGS), Subcommission on the Systematics of Igneous Rocks. 2nd edition. Cambridge
700 University Press, Cambridge/UK: pp236
701 Le Roex AP, Dick HJB, Erlank AJ, Reid AM, Frey FA, Hart SR (1983). Geochemistry,
702 mineralogy and petrogenesis of lavas erupted along the south west Indian ridge between
703 the Bouvet triple junction and 11 degrees east. J Petrol 24: 267–318.
704 Li XY, Zheng JP, Ma Q, Xiong Q, Griffin WL, Lu JG (2014). From enriched to depleted mantle:
705 Evidence from Cretaceous lamprophyres and Paleogene basaltic rocks in eastern and
706 central Guangxi Province, western Cathaysia block of South China. Lithos 184–187; 300-
707 313.
708 Li B, Jiang SY, Zhang Q, Zhao HX, Zhao KD (2015). Geochemistry, geochronology and Sr–
709 Nd–Pb–Hf isotopic compositions of Middle to Late Jurassic syenite–granodiorite–dacite
710 in South China: Petrogenesis and tectonic implications. Gondwana Research 35: 217-237.
711 Ling MX, Wang FY, Ding X, Zhou JB, Sun WD (2011). Different origins of adakites from the
712 Dabie Mountains and the Lower Yangtze River Belt, eastern China: geochemical
713 constraints. Int Geol Rev 53: 727–740.
714 Liu SA, Li SG, He YS, Huang F (2010). Geochemical contrasts between early Cretaceous ore-
715 bearing and ore-barren high-Mg adakites in central-eastern China: implications for
716 petrogenesis and Cu–Au mineralization. Geochim Cosmochim Acta 74: 7160–7178.
717 Macpherson CG, Dreher ST, Thirlwall MF (2006). Adakites without slab melting: high-
718 pressure differentiation of island arc magma, Mindanao, the Philippines. Earth Planet Sci
719 Lett 243: 581–593.

720 Martin H, Smithies RH, Rapp R, Moyen JF, Champion D (2005). An overview of adakite,
721 tonalite–trondhjemite–granodiorite (TTG), and sanukitoid: relationships and some
722 implications for crustal evolution. Lithos 79: 1-24.
723 Maury RC, Defant MJ, Joron JL (1992). Metasomatism of the sub-arc mantle inferred from
724 trace elements in Philippine xenoliths. Nature 360: 661–663.
725 McCall GJH (1997). The geotectonic history of the Makran and adjacent areas of southern Iran.
726 J Southeast Asian Earth Sci 15: 517–531.
727 McDonough WF, Sun SS (1995). The composition of the Earth. Chem Geol 120, 223–253.
728 Middlemost EAK (1972). A simple classification of volcanic rocks. Bull Volc 36, 382–397.
729 Morimoto N, Fabries J, Ferguson AK, Ginzburg IV, Ross M, Seifert FA, Zussman J, Aoki K,
730 Gottardi G (1988) Nomenclature of pyroxenes. Am Mineral 73:1123-1133
731 Moyen JF (2009). High Sr/Y and La/Yb ratios: The meaning of the "adakitic signature". Lithos
732 112, 556–574.
733 Müller D, Groves DI (2016; eds). Potassic igneous rocks and associated gold-copper
734 mineralization. Mineral Resource Reviews. 4th Edition. Springer Int Publ AG Cham/CH,
735 311pp.
736 Nachit HA, Abia EH, Ohoud MB (2005). Discrimination between primary magmatic biotites,
737 reequilibrated biotites and neoformed biotites. Comptes Rendus Geosci. 337: 1415–1420.
738 Nakamura N (1974). Determination of REE, Ba, Fe, Mg, Na and K in carbonaceous and
739 ordinary chondrites. Geochim Cosmochim Acta 38: 757–775.
740 Pang KN, Chung SL, Zarrinkoub MH, Khatib MM, Mohammadi SS, Chiu HY, Chu CH, Lee
741 HY, Lo CH (2013). Eocene–Oligocene post-collisional magmatism in the Lut–Sistan
742 region, eastern Iran: magma genesis and tectonic implications. Lithos 180–181: 234–251.
743 Parker DF (1983). Origin of the trachyte– quartz trachyte– peralkalic rhyolite suite of the
744 Oligocene Paisano volcano, Trana- Pecos Texas. Geol Soc Am, Bull 94, 614–629.

745 Pla Cid PJ, Nardi LVS, Conceicao H, Bonin B, Jardim DE SÁ E (2000). The alkaline silica-
746 saturated ultrapotassic magmatism of the Riacho do Pontal Fold Belt, NE Brazil: an
747 example of syenite-granite Neoproterozoic association. J South Am Earth Sci 13: 661–
748 683.
749 Plank T, Langmuir CH (1998). The chemical composition of subducting sediment and its
750 consequences for the crust and mantle. Chem Geol 145: 325–394.
751 Prelevic D, Foley SF (2007). Accretion of arc-oceanic lithospheric mantle in the Mediterranean:
752 evidence from extremely high-Mg olivines and Cr-rich spinel inclusions in lamproites.
753 Earth Planet Sci Lett 256: 120–135.
754 Rapp RP, Shimizu N, Norman MD (2003). Growth of early continental crust by partial melting
755 of eclogite. Nature 425: 605– 609.
756 Rapp RP, Watson EB, (1995). Dehydration melting of metabasalt at 8-32 kbar: Implications for
757 continental growth and crust-mantle recycling: Journal of Petrology 36: 891–931.
758 Rapp RP, Xiao L, Shimizu N (2002). Experimental constraints on the origin of potassium-rich
759 adakite in east China. Acta Petrol Sinica 18: 293–311.
760 Ribbe PH (1983) Chemistry, structure and nomenclature of feldspars. In: Ribbe PH (edr):
761 Feldspar mineralogy. 2nd edition. Rev Mineral 2:1-19
762 Richards JP, Spell T, Rameh E, Razique A, Fletcher T (2012). High Sr/Y magmas reflect arc
763 maturity, high magmatic water content, and porphyry Cu ± Mo ± Au potential: examples
764 from the Tethyan arcs of central and eastern Iran and western Pakistan. Econ Geol 107:
765 295–332.
766 Richards JP (2015). Tectonic, magmatic, and metallogenic evolution of the Tethyan orogen:
767 From subduction to collision. Ore Geol Rev 70(2):323–345.
768 Richards JP, Kerrich R (2007). Adakite-Like Rocks: Their Diverse Origins and Questionable
769 Role in Metallogenesis. Econ Geol 102: 537–576.

Rieder M, Cavazzini G, D'yakonov YS, Frank-Kamenetskii VA, Gottardi G, Guggenheim S, Koval PV, Müller G, Neiva AMR, Radoslovich EW, Robert JL, Sassi FP, Takeda H, Weiss Z, Wones DR (1998) Nomenclature of the micas. Clays Clay Minerals 46(5):586-595

Rogers NW, Hawkesworth CJ, Mattey DP, Harmon RS (1987). Sediment subduction and the source of potassium in orogenic leucitites. Geol 15: 451–453.

Rogers N, James D, Kelley S, DeMulder M (1998). The generation of potassic lavas from the eastern Virunga province, Rwanda. J Petrol 39: 1223–1247.

Rudnick RL (1995). Making continental crust. Nature 378: 571–578.

Rudnick RL, Fountain DM (1995). Nature and composition of the continental crust: a lower crustal perspective. Rev Geophys 33 (3): 267-309.

Rudnick RL, Gao S (2003). Composition of the continental crust. In: Holland H.D., Turekian K.K., (Eds.), Treatise on Geochemistry 3, The crust. Elsevier Pergamon Oxford. 1–64.

Scarrow JH, Bea F, Montero P, Molina JF (2009). Shoshonites, vaugnerites and potassic lamprophyres: similarities and differences between 'ultra' high-K rocks. Earth Env Sci, Trans Roy Soc Edinburgh 99: 159–175.

Schreiber HD, Lauer HV, Thanyasir T (1980). The redox state of cerium in basaltic magmas: an experimental study of iron–cerium interaction in silicate melts. Geochim Cosmochim Acta 44: 1599–1612.

Shao JA, Lu FX (2008). Re-discussion on the origin of volcanic rocks of the Xinglonggou Formation, North China. Acta Petrol Sinica 24: 1313–1322.

Sobolev AV, Hofmann AW, Kuzmin DH, Yaxley GM (2007). The amount of recycled crust in sources of mantle-derived melts. Sci 316: 412–417.

Stolz AJ, Jochum KP, Spettel B, Hofmann AW (1996). Fluid- and melt-related enrichment in the subarc mantle: evidence from Nb/Ta variations in island-arc basalts. Geol 24: 587–590.

796 Sun M, Kerrich R (1995). Rare earth element and high field strength element characteristics of
797 whole rocks andmineral separates of ultramafic nodules in Cenozoic volcanic vents of
798 southeastern British Columbia, Canada. Geochim Cosmochim Acta 59: 4863–4879.
799 Sun SS, Mc Donough WF (1989). Chemical and isotopic systematics of oceanic basalts:
800 implications for mantle compositions and processes. In: Saunders AD, Norry MJ (eds),
801 Magmatism in the Ocean Basins. Geol Soc London, Spec Publ 42: 313–345.
802 Tappe S, Foley SF, Jenner GA, Heaman LM, Kjarsgaard BA, Romer RL, Stracke A, Joyce N,
803 Hoefs J (2006). Genesis of ultramafic lamprophyres and carbonatites at Aillik Bay,
804 Labrador: a consequence of incipient lithospheric thinning beneath the North Atlantic
805 craton. J Petrol 47: 1261–1315.
806 Taylor SR, McLennan SM (1985). The continental crust: its composition and evolution.
807 Blackwell Scientific Publications, Oxford/UK, 312 pp.
808 Taylor SR, McLennan SM (1995). The geochemical evolution of the continental crust. Rev
809 Geophys 33: 241–265.
810 Thompson RN, Dickin AP, Gibson IL, Marrison MA (1982). Elemental fingerprints of isotopic
811 contamination of Hebridean Paleocene mantle-derived magmas by Archean sial. Contr
812 Mineral Petrol 79: 159-168.
813 Wang Q, Xu JF, Jian P, Bao ZW, Zhao ZH, Li CF, Xiong XL, Ma JL (2006). Petrogenesis of
814 adakitic porphyries in an extensional tectonic setting, Dexing, South China: implications
815 for the genesis of porphyry copper mineralization. J Petrol 47: 119–144.
816 Wang Q, Wyman DA, Xu JF, Jian P, Zhao ZH, Li CF, Xu W, Ma JL, He B (2007). Early
817 Cretaceous adakitic granites in the Northern Dabie Complex, Central China: implications
818 for partial melting and delamination of thickened lower crust. Geochim Cosmochim Acta
819 71: 2609–2636.

820 Woodard J, Kietäväinen R, Eklund O (2014). Svecofennian post-collisional shoshonitic
821 lamprophyres at the margin of the Karelia Craton: Implications for mantle metasomatism.
822 Lithos 205: 379–393.
823 Yang J, Godard G, Kienast JR, Lu Y, Sun J (1993). Ultra high pressure 60 kbar magnesite-
824 bearing garnet peridotites from northeastern Jiangsu, China. J Geol 101: 541– 554.
825 Yogodzinski GM, Kay RW, Volynets ON, Koloskov AV, Kay SM, (1995). Magnesian andesite
826 in the western Aleutian Komandorsky region: implications for slab melting and processes
827 in the mantle wedge. Geol Soc Am, Bull 107: 505–519.
828 Zhang RY, Liou JG, Cong B (1994). Petrogenesis of garnetbearing ultramafic rocks and
829 associated eclogites in the SuLu ultrahigh-P metamorphic terrane, eastern China. J Metam
830 Geol 12: 169–186.
831 Zhang Z, Xiao X, Wang J, Wang Y, Kusky TM (2008). Post-collisional Plio- Pleistocene
832 shoshonitic volcanism in the western Kunlun Mountains, NW China: geochemical
833 constraints on mantle source characteristics and petrogenesis. J Asian Earth Sci 31: 379–
834 403.

Figure captions

Fig 1. Simple geological map of Lar igneous suite (LIS) in the Sistan suture zone in southeastern Iran, showing important lithological and structural units. UDMB: Urmieh-Dokhtar Magmatic Belt.

Fig 2. Cross nicols light photomicrographs of: (a) Microphenocrysts of lath shape plagioclase with parallel orientation along crystallographic surface of the host K-feldspar megacrystes; (b) kink-band microtexture in biotite and k-feldspar overgrowth on plagioclase, showing anti-rapakivi texture (red arrow point to k-feldspar overgrowth). Bt: Biotite; Kfs: K-feldspar; Pl: Plagioclase.

Fig 3. Fo vs. Ni (ppm) for olivines in the LIS syenites. Data sources for olivines in: Hawaii (Sobolev et al., 2007), MORB (Sobolev et al., 2007), Mediterranean (Prelevic and Foley, 2007).

Fig 4. Al vs. Ti diagram for clinopyroxenes in the LIS syenites (after Conticelli et al., 1997), diagnosing Roman type clinopyroxenes (orogenic) from transition and Lamproitic (intra plate) types. a.f.u=atoms per formula unit.

Fig 5. (a) Mg-(AlVI+Fe3++Ti)-(Fe2++Mn) triangle diagram (after Forster 1960); and (b) 10*TiO2-(FeO+MnO)-MgO ternary plot for micas in the LIS syenites (after Nachit et al. 2005).

Fig 6. (a) Chondrite normalized REE patterns (Nakamura, 1974); and (b) Primitive mantle-normalized multi element diagrams (McDonough and Sun, 1995) for LIS syenites.

Fig 7. Major elements chemical variation diagrams for LIS syenites.

Fig 8. (a) K_2O/Na_2O vs. SiO_2; (b) La/Yb vs. SiO_2; (c) La/Yb vs. La (ppm); and (d) La/Sm vs. La (ppm) diagrams for the LIS syenites (after Li et al., 2015).

Fig 9. (a) TiO2 vs. total Fe2O3 and (b) Ba/Zr vs. Nb/Zr diagram for the LIS syenites. Fields of fertile and refractory peridotitic melts from Falloon et al. (1988); Roman Province from Conticelli et al. (1997), Tibetan Plateau from Turner et al. (1996), Rio Grande rift flank

from Gibson et al. (1993), MORB from Le Roex et al. (1983) and OIB from Chaffey et al. (1989).

Fig 10. (a) Adakite classification diagram for LIS syenites. Fields of adakite and normal andesite-dacite-rhyolite are after Richards and Kerrich (2007), and (b) Sr/Y vs. (La/Yb)N diagram (after Liu et al., 2010). LCC: lower continental crust.

Fig 11. (a) Sr/Nb vs. Gd/Yb; and (b) Rb/Sr vs. Sr/Y for the adakitic syenites in the LIS (after Gao et al., 2010).

Fig 12. (a) Cr (ppm) vs. SiO2; (b) Ni (ppm) vs. SiO2; (c) Rb/Sr vs. Ba/Sr diagram (after Rogers et al., 1987), and, (d) Rb/Sr vs. Ba/Rb diagram (after Furman and Graham, 1999) for the LIS adakitic syenites. The field for subducted oceanic crust-derived adakites is from Defant and Kepezhinskas (2001), the fields for delaminated lower crust and thick lower crust-derived adakite-like rocks are from Wang et al. (2006); values for OIB and MORB are from Sun and McDonough (1989).

Table captions

Table 1 – Main element oxide contents in wt% in selected olivine grains from LIS syenites, by EPMA. FeO^T represents total iron (oxide) content. Numbers of cations in apfu calculated following guidance by Deer et al. (2013).

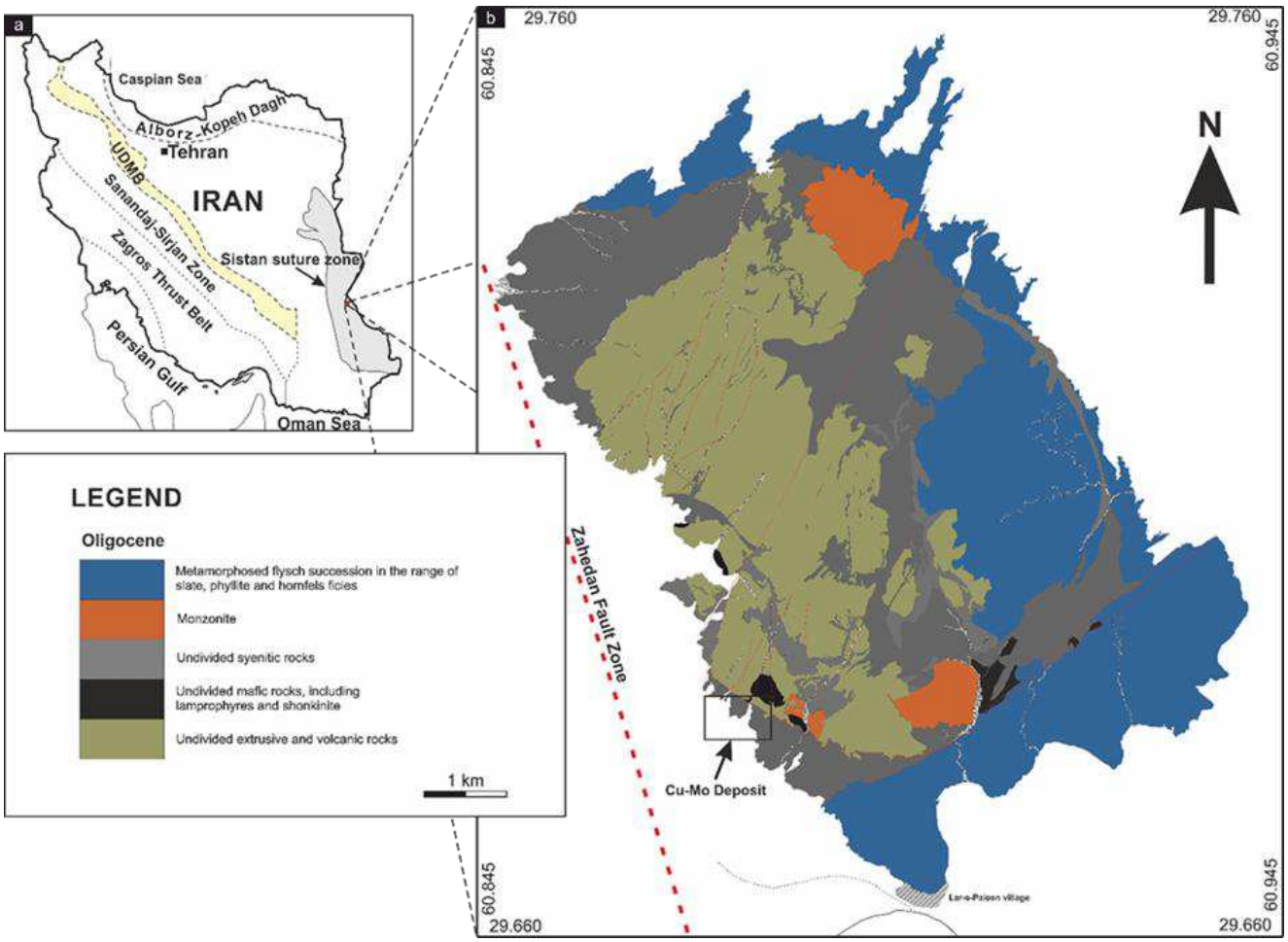
Table 2 – Main element oxide contents in wt% in selected clinopyroxene grains from LIS syenites, by EPMA. FeO^T represents total iron (oxide) content. Numbers of cations in apfu calculated following guidance of Morimoto et al. (1988).

Table 3 – Main element oxide contents in wt% in selected mica grains from LIS syenites, by EPMA. FeO^T represents total iron (oxide) content. Numbers of cations in apfu calculated following guidance of Rieder et al. (1998).

Table 4 – Main element oxide contents in wt% in selected feldspar grains from LIS syenites, by EPMA. $Fe_2O_3^T$ represents total iron (oxide) content. Numbers of cations in apfu calculated based on 8O, following guidance of Ribbe (1983).

Table 5 – Main element oxide contents in wt%, trace elements and rare-earth elements (REE) in parts per million (ppm; µg·g-1) in adakitic syenites from LIS, by ICP-MS (LOI gravimetric). $Fe_2O_3^T$ represents total iron (oxide) content.

Figures



Figure

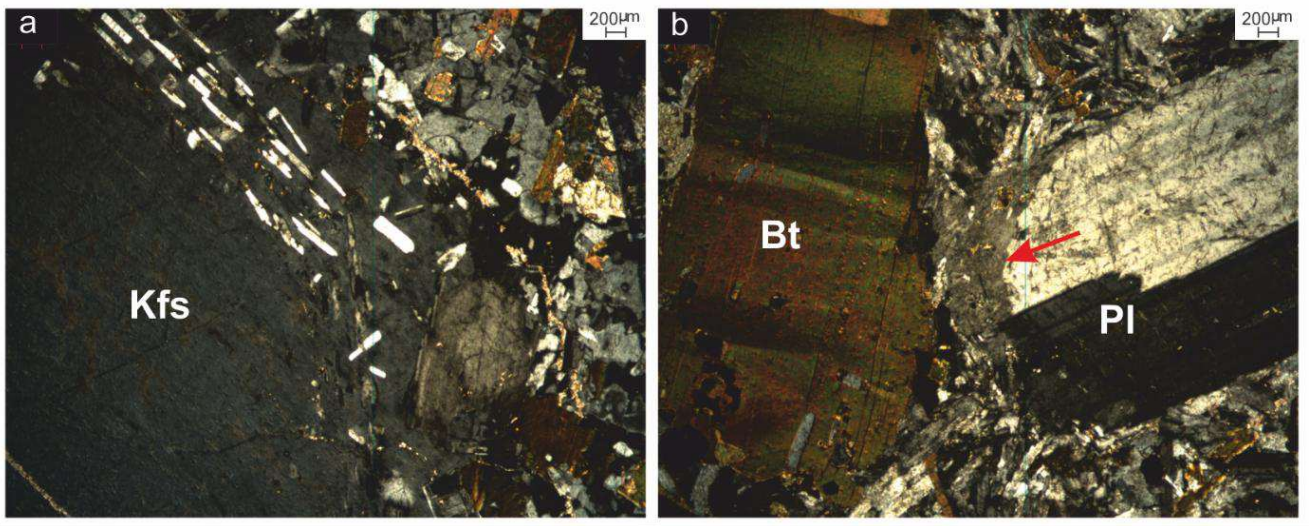


Figure 2

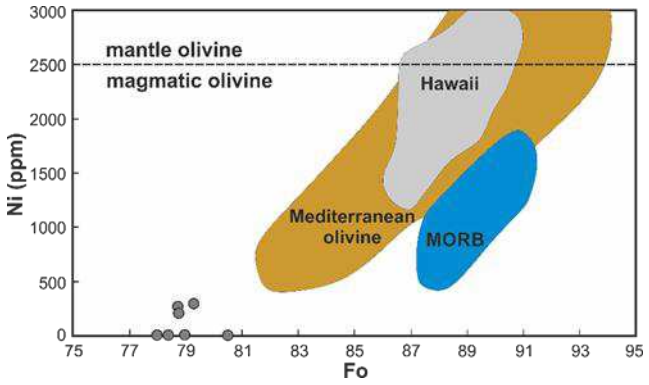
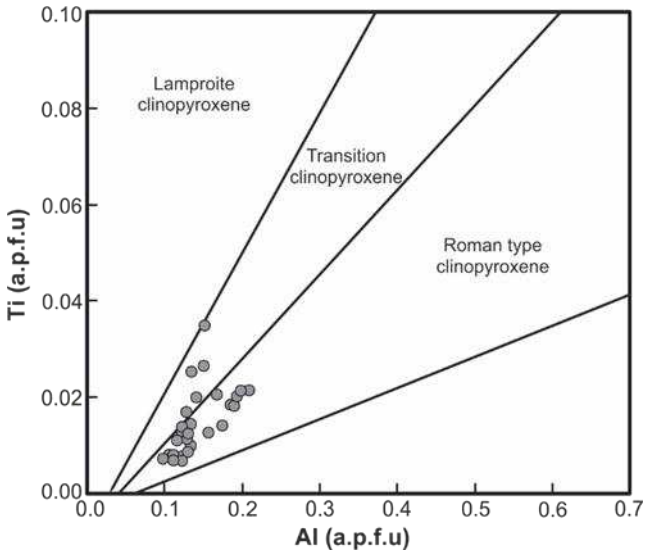
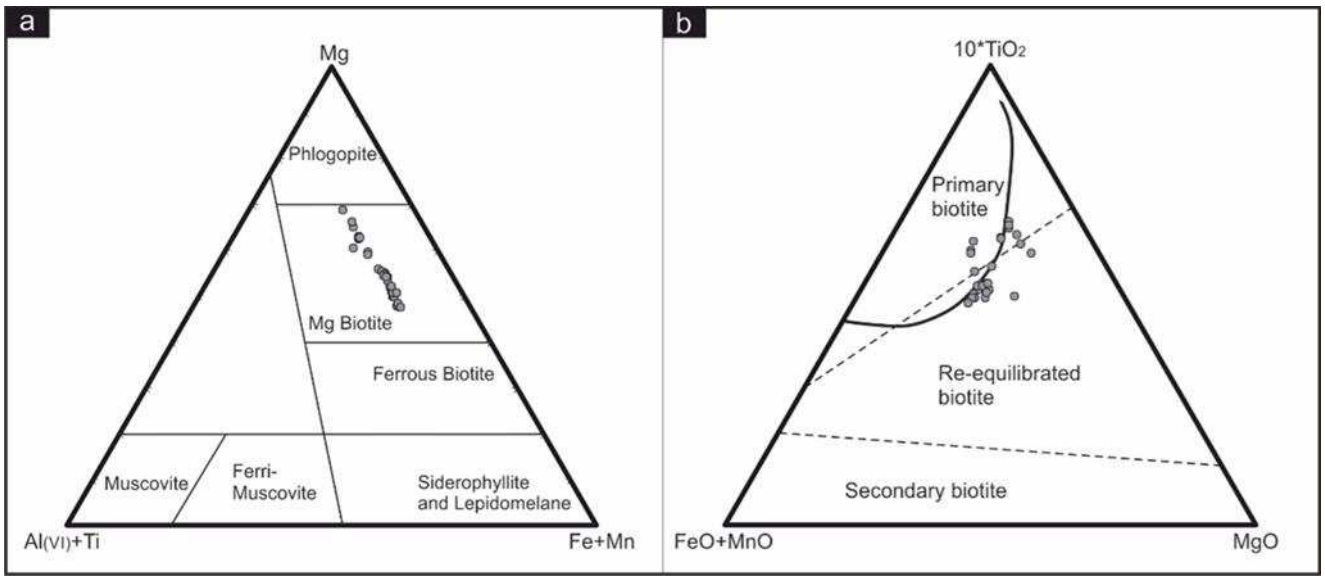

mantle olivine
magmatic olivine
Hawaii
Mediterranean olivine
MORB
Ni (ppm)
Fo
3000
2500
2000
1500
1000
500
0
75
77
79
81
83
85
87
89
91
93
95

Figure 3



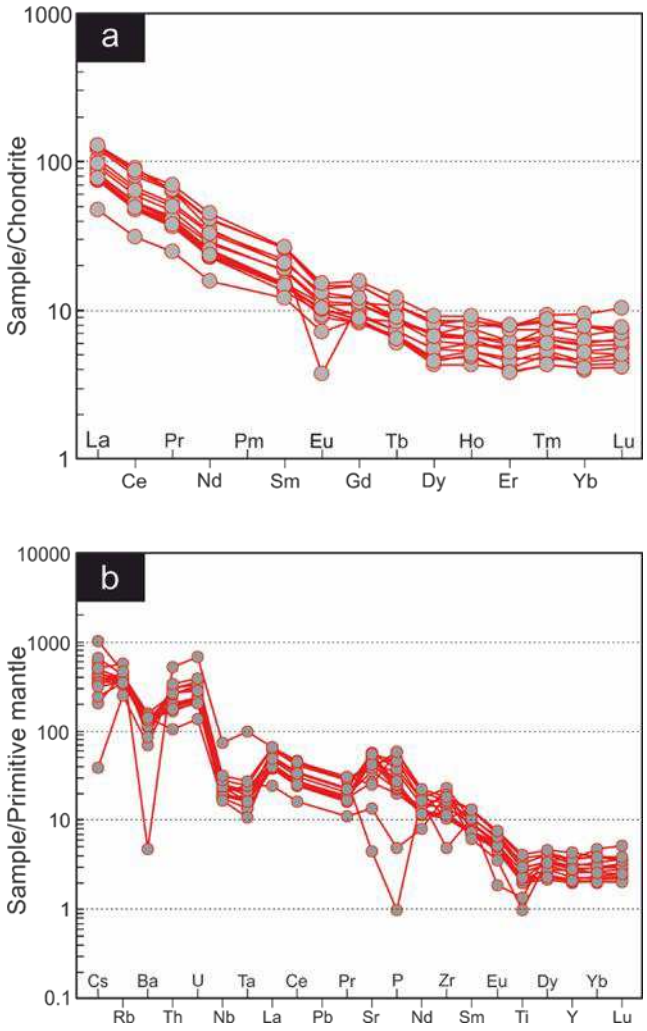
898

899 Figure 4



900

901 Figure 5



902

903 Figure 6

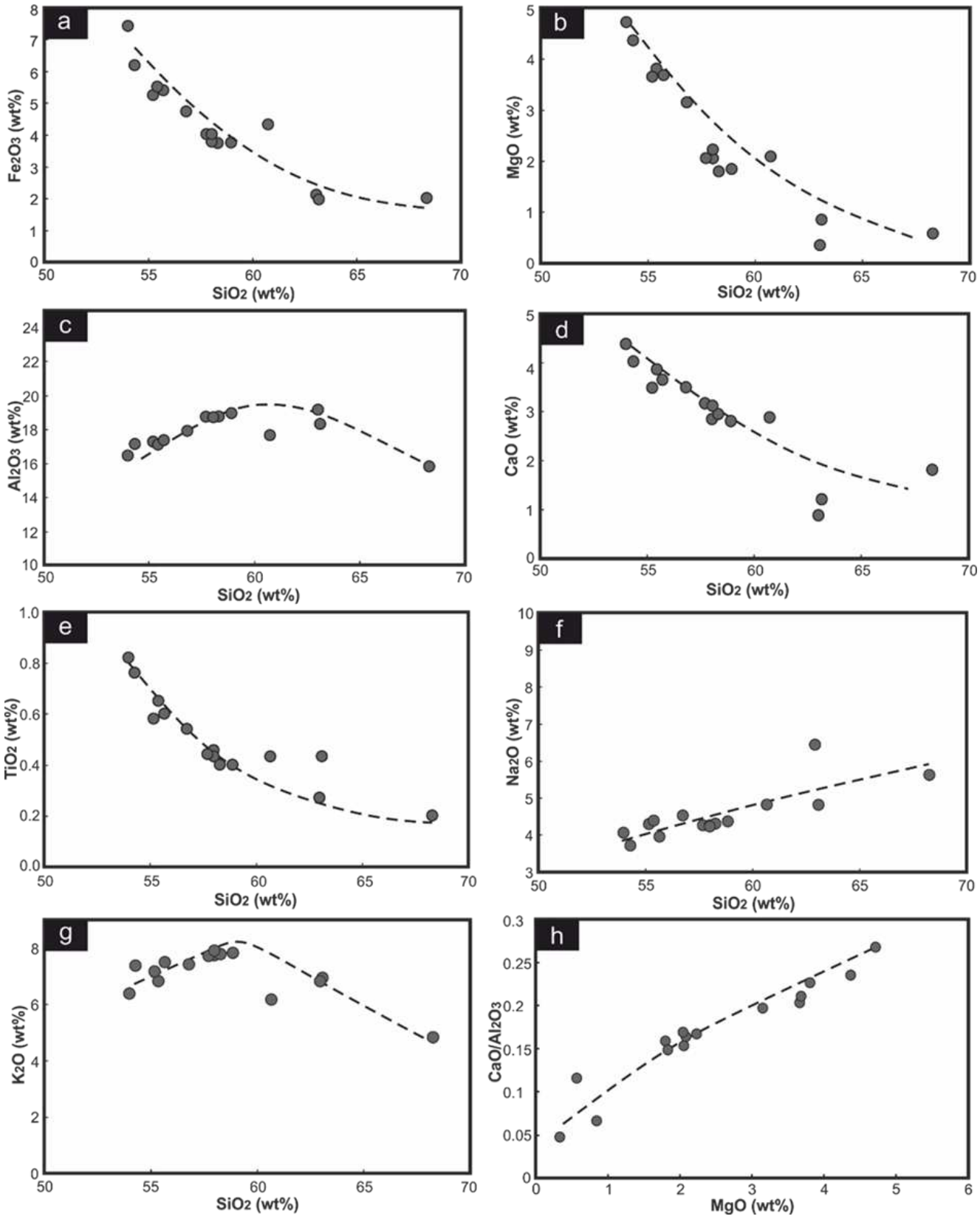

a
Fe2O3 (wt%)
SiO2 (wt%)
b
MgO (wt%)
SiO2 (wt%)
c
Al2O3 (wt%)
SiO2 (wt%)
d
CaO (wt%)
SiO2 (wt%)
e
TiO2 (wt%)
SiO2 (wt%)
f
Na2O (wt%)
SiO2 (wt%)
g
K2O (wt%)
SiO2 (wt%)
h
CaO/Al2O3
MgO (wt%)

Figure 7

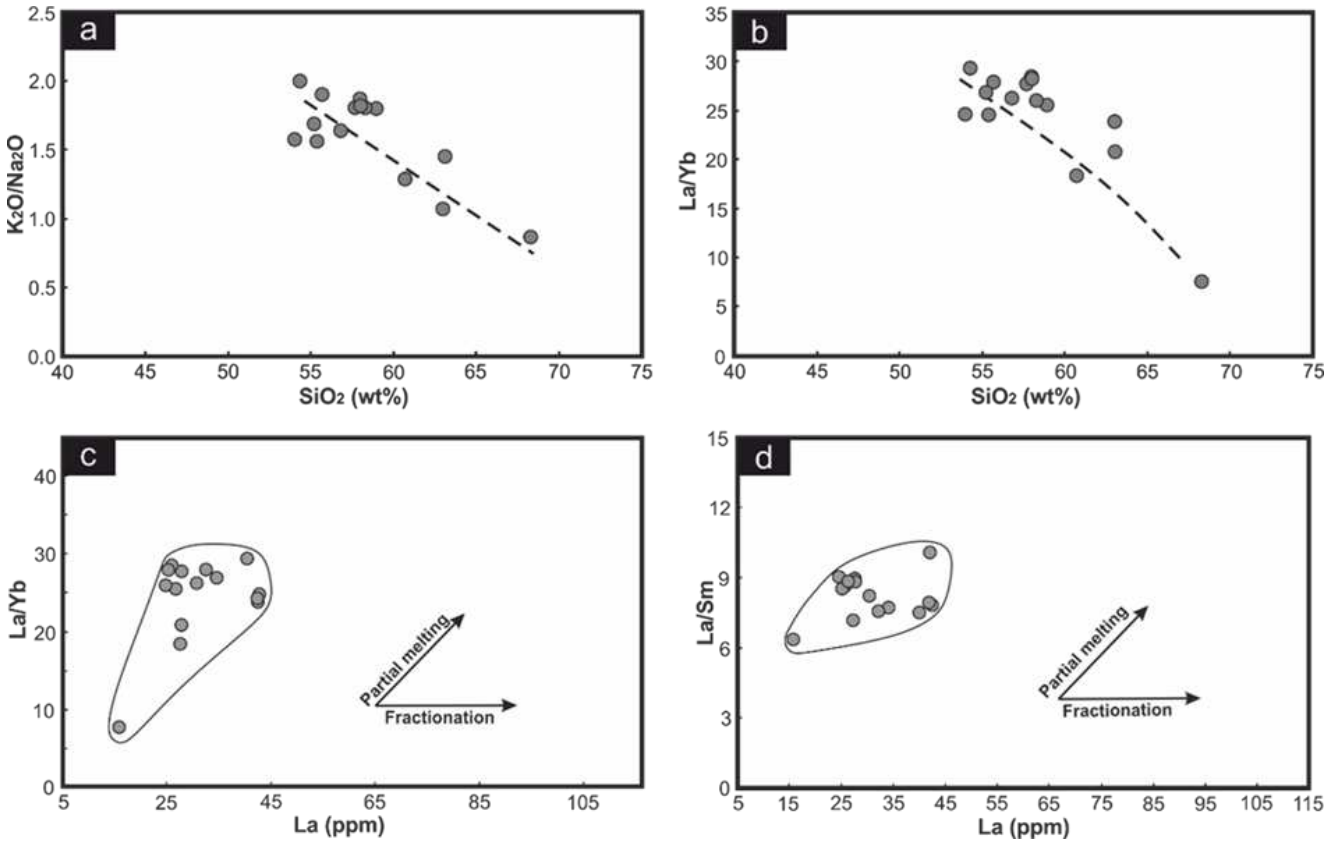
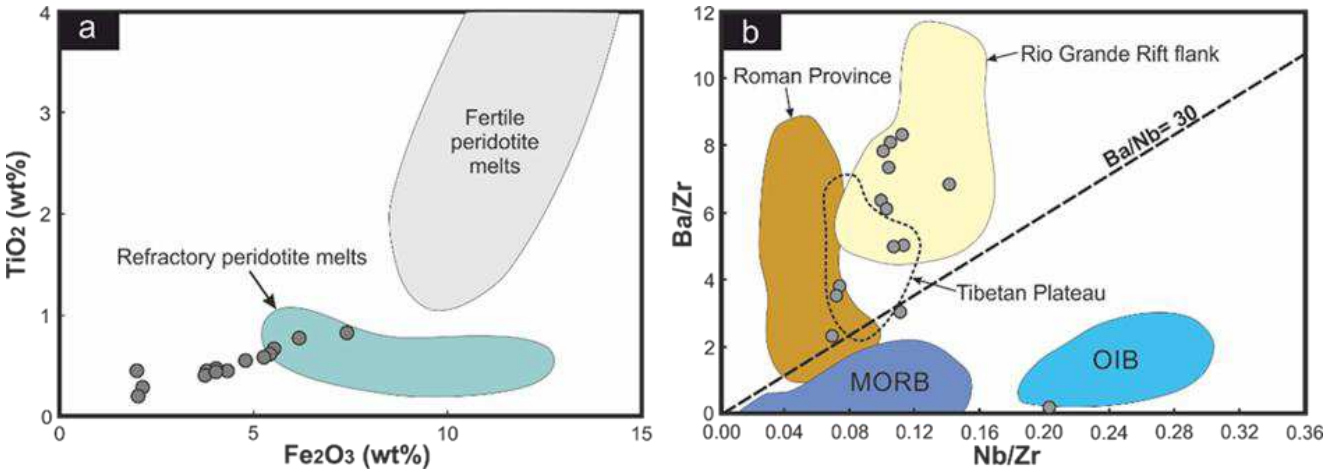
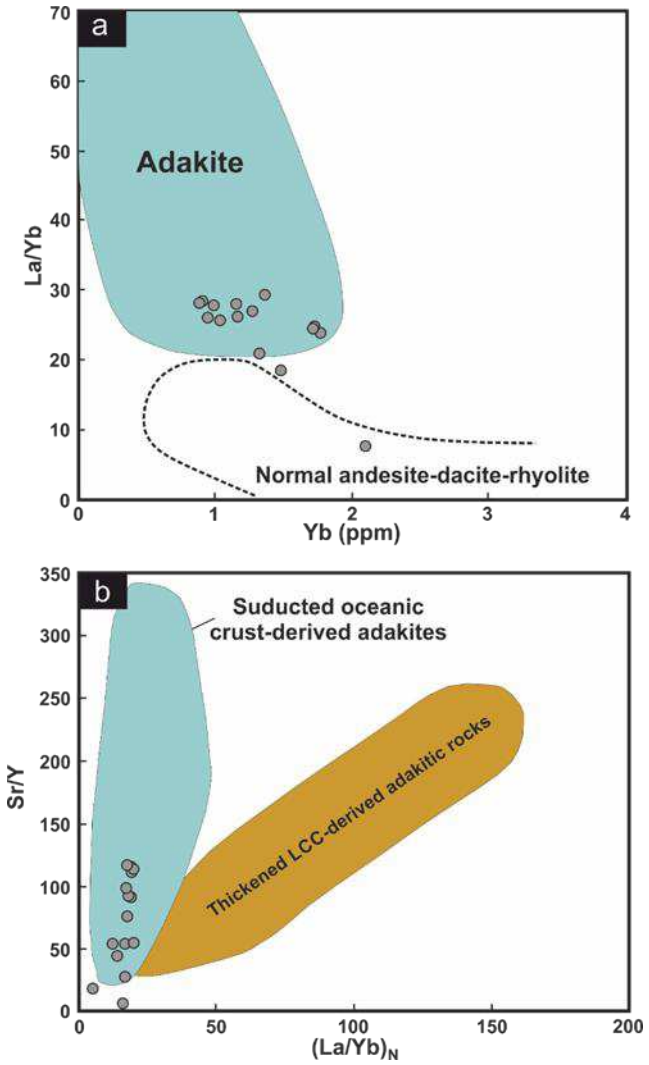

a
b
c
d
K2O/Na2O
SiO2 (wt%)
La/Yb
La/Sm
La (ppm)
Partial melting
Fractionation

Figure 8



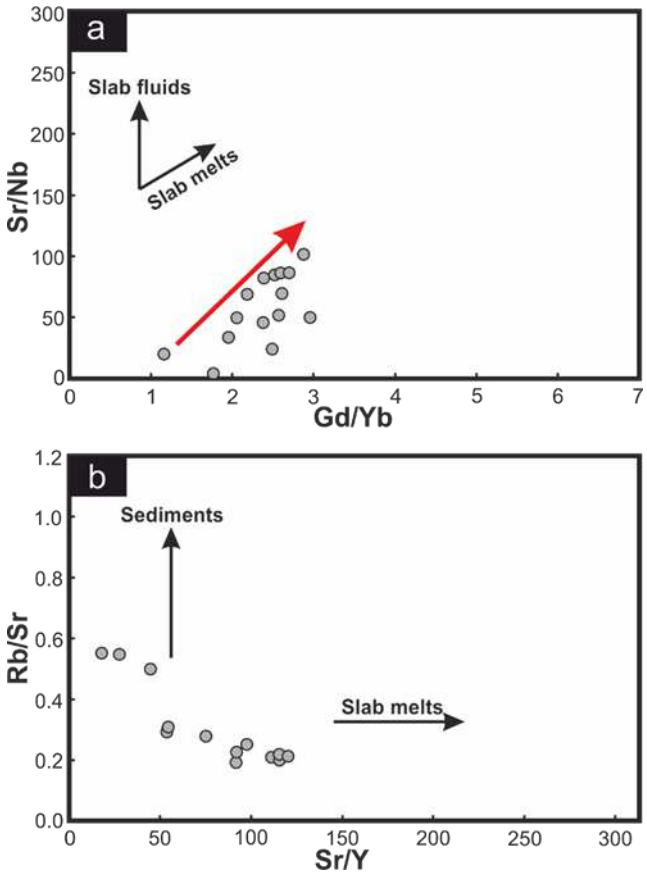
908

909 Figure 9



910

911 Figure 10



912

913 Figure 11

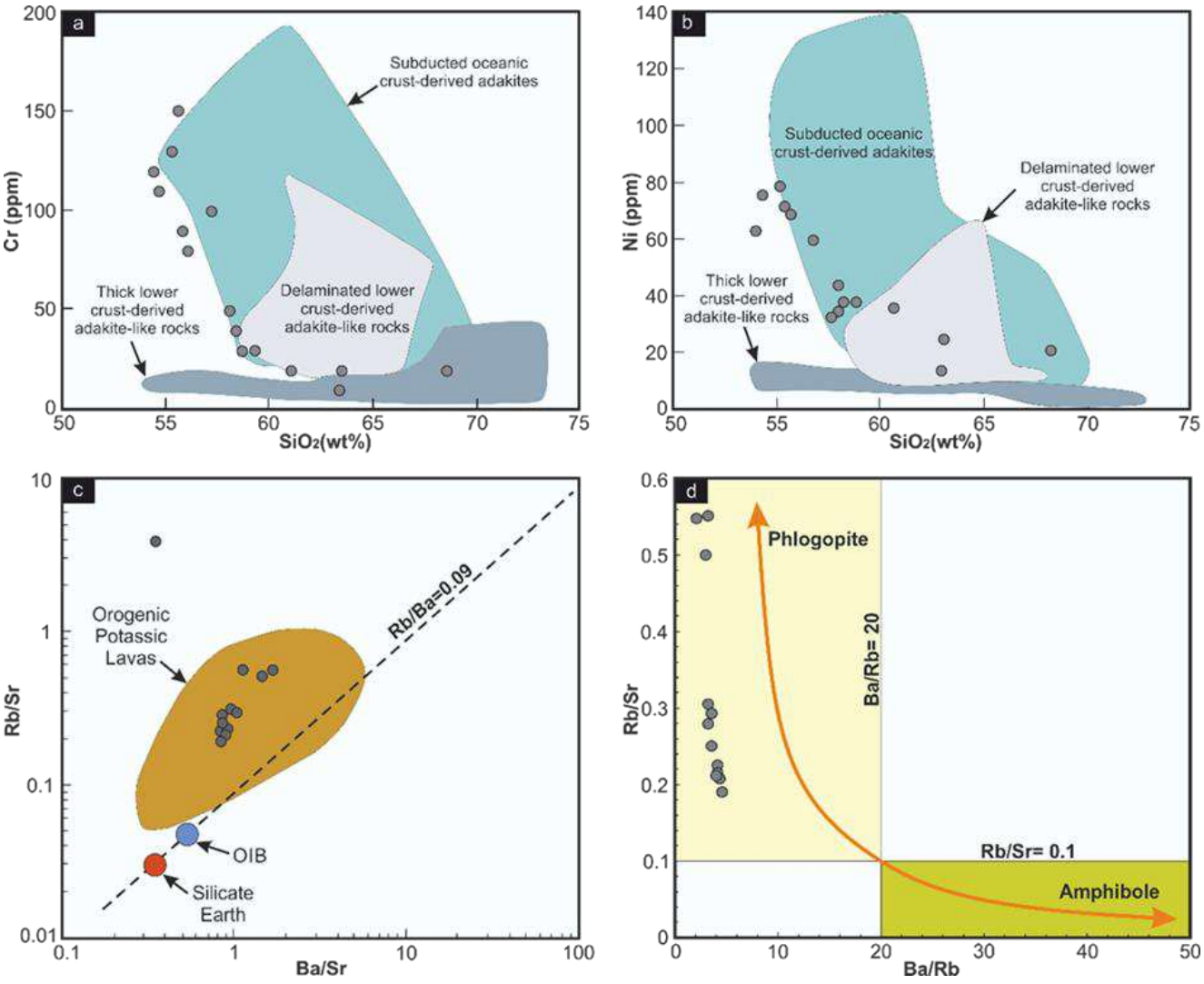

a
Subducted oceanic crust-derived adakites
Thick lower crust-derived adakite-like rocks
Delaminated lower crust-derived adakite-like rocks
Cr (ppm)
SiO2(wt%)
b
Subducted oceanic crust-derived adakites
Delaminated lower crust-derived adakite-like rocks
Thick lower crust-derived adakite-like rocks
Ni (ppm)
SiO2(wt%)
c
Orogenic Potassic Lavas
Rb/Ba=0.09
OIB
Silicate Earth
Rb/Sr
Ba/Sr
d
Phlogopite
Ba/Rb= 20
Rb/Sr= 0.1
Amphibole
Rb/Sr
Ba/Rb

Figure 12

Tables

Table 1 – Main element oxide contents in wt% in selected olivine grains from LIS syenites, by EPMA. FeO^T represents total iron (oxide) content. Numbers of cations in apfu calculated following guidance by Deer et al. (2013)

spot	LLD(wt%)	1	2	3	4	5	6	7
		main element oxide contents in weight percent (wt%)						
SiO_2	0.01	38.22	37.31	38.42	38.56	38.01	38.19	37.99
TiO_2	0.01	<LLD	0.03	<LLD	<LLD	<LLD	0.01	0.01
Al_2O_3	0.01	0.01	0.11	0.01	0.02	0.02	0.06	0.23
Cr_2O_3	0.01	<LLD	0.04	<LLD	0.03	0.04	<LLD	<LLD
FeO^T	0.01	17.28	18.08	18.40	18.63	18.61	19.05	19.03
MnO	0.01	0.77	1.04	0.98	1.04	1.14	1.08	1.08
NiO	0.01	0.13	0.09	0.11	0.07	0.08	0.04	0.14
MgO	0.01	42.37	41.63	41.16	41.43	41.45	41.37	40.46
CaO	0.01	0.13	0.14	0.06	0.14	0.10	0.11	0.14
Na_2O	0.01	0.07	0.14	0.14	0.12	0.11	0.15	0.16
Total		98.98	98.61	99.28	100.04	99.56	100.06	99.24
		numbers of cations in atoms per formula unit (apfu) on the basis of 4O						
Si	-	0.986	0.974	0.994	0.991	0.983	0.984	0.987
Σ *T*		0.986	0.974	0.994	0.991	0.983	0.984	0.987
Ti	-	0.000	0.001	0.000	0.000	0.000	0.000	0.000
Al	-	0.000	0.002	0.000	0.000	0.000	0.001	0.004
Cr	-	0.000	0.000	0.000	0.000	0.000	0.000	0.000
Fe^{2+}	-	0.373	0.395	0.398	0.400	0.403	0.410	0.414
Mn	-	0.017	0.023	0.021	0.023	0.025	0.024	0.024
Ni	-	0.003	0.002	0.002	0.002	0.002	0.001	0.003
Mg	-	1.630	1.620	1.587	1.587	1.598	1.589	1.567
Ca	-	0.004	0.004	0.002	0.004	0.003	0.003	0.004
Na	-	0.002	0.004	0.003	0.003	0.003	0.004	0.004
Σ *M*		2.029	2.051	2.013	2.019	2.034	2.032	2.020
sum cations		3.015	3.025	3.007	3.010	3.017	3.016	3.007
		calculated forsterite content (mol%)						
Fo	-	80.6	79.4	79.0	78.8	78.8	78.4	78.0

Table 2 – Main element oxide contents in wt% in selected clinopyroxene grains from LIS syenites, by EPMA. FeO^T represents total iron (oxide) content. Numbers of cations in apfu calculated following guidance of Morimoto et al. (1988)

spot	LLD(wt%)	1	2	3	4	5	6	7	8	9	10	11	12	13	14	15	16	17	18	19	20
main element oxide contents in weight percent (wt%)																					
SiO^2	0.01	49.31	50.33	50.78	51.10	51.07	51.51	50.83	50.19	49.66	52.26	50.26	51.16	50.28	50.95	50.20	49.94	50.50	50.83	50.53	50.83
Al_2O_3	0.01	4.17	3.56	2.97	2.79	2.97	2.63	2.74	4.32	4.35	2.95	3.45	3.07	3.43	2.77	4.50	3.77	2.54	2.72	2.54	2.19
TiO_2	0.01	0.66	0.48	0.44	0.46	0.41	0.39	0.24	0.65	0.71	0.61	1.24	0.91	0.94	0.49	0.76	0.73	0.28	0.26	0.24	0.26
Cr_2O_3	0.01	0.22	0.16	0.11	0.11	0.12	0.08	<LLD	0.14	0.22	0.04	0.05	<LLD	0.10	0.23	0.11	0.17	0.08	<LLD	<LLD	0.05
NiO	0.01	0.03	0.02	<LLD	0.02	<LLD	0.01	0.01	0.01	0.03	0.05	<LLD	0.02	<LLD	0.03	0.00	<LLD	<LLD	<LLD	<LLD	0.02
FeO^T	0.01	6.56	6.78	6.59	6.67	6.60	6.11	9.07	7.12	6.49	6.28	6.05	6.13	6.41	6.35	7.23	6.52	7.11	7.31	7.32	8.21
MnO	0.01	0.17	0.21	0.21	0.30	0.24	0.19	0.41	0.21	0.21	0.32	0.24	0.21	0.24	0.20	0.18	0.24	0.25	0.38	0.37	0.39
MgO	0.01	15.28	14.32	15.49	15.32	15.63	15.06	12.58	14.71	14.52	14.35	14.67	14.88	14.64	14.62	15.10	14.50	14.62	14.08	14.37	13.38
CaO	0.01	20.93	22.38	21.90	22.30	21.92	22.46	22.44	21.07	21.15	22.02	21.92	22.10	21.49	22.01	20.42	21.44	22.94	22.60	22.71	22.37
K_2O	0.01	0.19	0.02	<LLD	<LLD	0.01	<LLD	0.01	<LLD	<LLD	0.02	0.02	0.03	0.15	0.02	0.02	0.02	<LLD	<LLD	0.02	0.01
Na_2O	0.01	1.10	0.98	0.62	0.69	0.64	0.63	0.94	1.01	1.19	1.30	1.06	1.19	1.16	1.10	1.09	1.21	0.87	0.98	0.76	0.95
Total		98.62	99.24	99.11	99.76	99.61	99.07	99.27	99.43	98.53	100.20	98.96	99.70	98.84	98.77	99.61	98.54	99.19	99.16	98.86	98.66
numbers of cations in atoms per formula unit (apfu) on the basis of 6O																					
Si		1.857	1.887	1.899	1.902	1.900	1.923	1.924	1.873	1.869	1.929	1.882	1.901	1.888	1.914	1.867	1.881	1.901	1.913	1.909	1.930
Al^{IV}		0.143	0.113	0.101	0.098	0.100	0.077	0.076	0.127	0.131	0.071	0.118	0.099	0.112	0.086	0.133	0.119	0.099	0.087	0.091	0.070
Σ T		2.000	2.000	2.000	2.000	2.000	2.000	2.000	2.000	2.000	2.000	2.000	2.000	2.000	2.000	2.000	2.000	2.000	2.000	2.000	2.000
Al^{VI}		0.043	0.045	0.030	0.025	0.030	0.038	0.046	0.063	0.062	0.058	0.035	0.036	0.040	0.036	0.065	0.049	0.013	0.033	0.022	0.028
Ti		0.019	0.013	0.012	0.013	0.011	0.011	0.007	0.018	0.020	0.017	0.035	0.025	0.027	0.014	0.021	0.021	0.008	0.007	0.007	0.007
Cr		0.007	0.005	0.003	0.003	0.004	0.002	0.000	0.004	0.007	0.001	0.001	0.000	0.003	0.007	0.003	0.005	0.002	0.000	0.000	0.002
Fe^{2+}		0.181	0.197	0.184	0.188	0.183	0.176	0.273	0.195	0.183	0.182	0.174	0.176	0.183	0.185	0.193	0.186	0.209	0.216	0.216	0.247
Mg		0.751	0.740	0.771	0.771	0.772	0.772	0.674	0.719	0.728	0.742	0.755	0.763	0.747	0.758	0.718	0.739	0.767	0.743	0.756	0.716
Σ M1		1.000	1.000	1.000	1.000	1.000	1.000	1.000	1.000	1.000	1.000	1.000	1.000	1.000	1.000	1.000	1.000	1.000	1.000	1.000	1.000
Fe^{2+}		0.026	0.016	0.022	0.019	0.022	0.015	0.014	0.027	0.022	0.012	0.015	0.014	0.018	0.015	0.032	0.019	0.015	0.014	0.015	0.014
Mg		0.107	0.060	0.093	0.079	0.095	0.066	0.036	0.099	0.086	0.048	0.064	0.062	0.072	0.060	0.119	0.075	0.054	0.047	0.053	0.041
Mn		0.006	0.007	0.007	0.009	0.007	0.006	0.013	0.007	0.007	0.010	0.008	0.006	0.008	0.006	0.006	0.008	0.008	0.012	0.012	0.012
Ca		0.845	0.899	0.878	0.889	0.874	0.898	0.910	0.842	0.853	0.871	0.880	0.880	0.865	0.886	0.814	0.865	0.925	0.911	0.919	0.910
Na		0.080	0.071	0.045	0.050	0.046	0.046	0.069	0.073	0.087	0.093	0.077	0.085	0.085	0.080	0.079	0.088	0.064	0.072	0.056	0.070
K		0.009	0.001	0.000	0.000	0.000	0.000	0.000	0.000	0.000	0.001	0.001	0.002	0.007	0.001	0.001	0.001	0.000	0.000	0.001	0.000
Σ M2		1.073	1.054	1.044	1.047	1.045	1.030	1.043	1.048	1.055	1.036	1.045	1.050	1.054	1.048	1.051	1.057	1.065	1.056	1.056	1.048
Total cations		4.073	4.054	4.044	4.047	4.045	4.030	4.043	4.048	4.055	4.036	4.045	4.050	4.054	4.048	4.051	4.057	4.065	4.056	4.056	4.048
calculated endmember proportions content (mol%)																					
Wo		44.2	47.0	45.1	45.7	44.9	46.6	47.7	44.8	44.7	45.6	45.0	46.6	46.5	45.9	46.5	43.4	47.0	47.2	46.9	47.2
En		44.9	41.9	44.4	43.7	44.6	43.5	37.2	44.0	43.5	43.5	43.6	43.4	43.5	43.5	43.0	44.6	41.7	40.9	41.3	39.3
Fs		10.8	11.1	10.6	10.7	10.6	9.9	15.1	11.2	11.8	10.9	11.4	10.0	10.1	10.7	10.5	12.0	11.4	11.9	11.8	13.5
sum		100.0	100.0	100.0	100.0	100.0	100.0	100.0	100.0	100.0	100.0	100.0	100.0	100.0	100.0	100.0	100.0	100.0	100.0	100.0	100.0
Mg#		80.6	79.0	80.7	80.4	80.9	81.5	71.2	79.7	78.6	80.0	79.3	81.2	81.2	80.3	80.4	78.8	78.6	77.4	77.8	74.4

Table 3 – Main element oxide contents in wt% in selected mica grains from LIS syenites, by EPMA. FeO^T represents total iron (oxide) content. Numbers of cations in apfu calculated following guidance of Rieder et al. (1998)

spot	**LLD**	**1**	**2**	**3**	**4**	**5**	**6**	**7**	**8**	**9**	**10**	**11**	**12**	**13**	**14**	**15**	**16**	**17**	**18**	**19**	**20**
										main element oxide contents in weight percent (wt%)											
SiO_2	0.01	36.71	36.12	36.16	36.18	36.55	36.79	36.55	36.76	36.09	36.79	37.06	37.51	36.63	36.63	36.54	37.38	37.37	38.28	38.36	37.02
TiO_2	0.01	3.13	3.26	3.48	3.27	3.39	3.48	3.50	3.23	3.27	3.15	4.73	4.69	4.92	3.76	2.98	3.89	4.82	4.03	4.51	5.46
Al_2O_3	0.01	14.07	13.88	14.63	14.46	14.55	14.40	14.12	14.19	14.28	14.12	14.88	14.93	14.00	14.42	14.72	14.40	14.67	14.63	14.38	14.20
Cr_2O_3	0.01	0.08	0.06	0.10	0.04	0.10	<LLD	<LLD	0.04	0.02	0.02	<LLD	0.04	<LLD	0.07	<LLD	0.04	0.06	0.29	<LLD	<LLD
FeO^T	0.01	17.41	17.75	16.85	16.57	16.99	15.73	15.79	15.31	15.99	16.44	12.36	12.56	17.45	16.97	18.32	14.63	10.25	8.69	10.13	11.03
MnO	0.01	0.31	0.28	0.27	0.27	0.28	0.31	0.31	0.31	0.33	0.40	0.14	0.21	0.40	0.28	0.29	0.26	0.16	0.06	0.09	0.08
MgO	0.01	13.98	13.95	14.35	14.04	13.87	15.09	15.21	15.19	14.94	15.39	15.53	15.53	12.56	13.14	13.21	15.26	17.71	19.08	18.40	16.82
CaO	0.01	<LLD	<LLD	<LLD	0.04	0.07	0.04	0.02	0.02	0.06	0.04	<LLD	0.04	<LLD	0.02	0.02	0.04	0.10	0.12	0.08	0.02
Na_2O	0.01	0.29	0.27	0.48	0.26	0.17	0.68	0.50	0.45	0.56	0.49	0.58	0.47	0.36	0.36	0.30	0.37	0.51	0.47	0.55	0.63
K_2O	0.01	9.80	9.37	9.43	9.64	9.77	9.58	9.61	9.56	9.50	9.46	9.19	9.48	9.85	9.53	9.66	9.57	9.72	9.79	9.53	9.60
F	0.01	0.19	0.12	0.09	0.14	0.10	0.38	0.32	0.14	0.04	0.15	0.43	0.26	0.10	0.25	0.30	0.18	0.31	0.09	0.80	0.68
Cl	0.01	0.01	0.02	0.02	0.03	0.04	0.02	0.03	0.03	0.02	0.02	0.04	0.01	0.03	<LLD	<LLD	0.03	0.09	0.07	0.07	0.08
H_2O	0.01	3.84	3.84	3.90	3.83	3.89	3.80	3.80	3.88	3.90	3.90	3.78	3.91	3.89	3.81	3.79	3.91	3.89	4.04	3.71	3.68
Total		99.82	98.92	99.76	98.77	99.77	100.30	99.76	99.11	99.00	100.37	98.72	99.64	100.19	99.24	100.13	99.96	99.66	99.64	100.61	99.30
										numbers of cations in atoms per formula unit (apfu) on the basis of 22O											
Si		5.524	5.489	5.424	5.479	5.487	5.471	5.469	5.513	5.443	5.476	5.490	5.508	5.496	5.525	5.497	5.528	5.449	5.527	5.532	5.451
Ti		0.000	0.000	0.000	0.000	0.000	0.000	0.000	0.000	0.000	0.000	0.000	0.000	0.000	0.000	0.000	0.000	0.000	0.000	0.000	0.000
Al^{IV}		2.527	2.517	2.620	2.613	2.606	2.556	2.522	2.540	2.570	2.508	2.631	2.616	2.507	2.595	2.642	2.542	2.554	2.521	2.475	2.495
Σ T		8.051	8.006	8.044	8.093	8.093	8.027	7.991	8.053	8.013	7.984	8.121	8.124	8.003	8.120	8.139	8.070	8.003	8.048	8.007	7.946
Al^{VI}		0.000	0.000	0.000	0.000	0.000	0.000	0.000	0.000	0.000	0.000	0.000	0.000	0.000	0.000	0.000	0.000	0.000	0.000	0.000	0.000
Ti		0.838	0.797	0.805	0.828	0.839	0.817	0.815	0.817	0.808	0.801	0.792	0.818	0.837	0.822	0.835	0.820	0.826	0.837	0.810	0.810
Fe		2.219	2.284	2.140	2.126	2.160	1.981	2.000	1.944	2.043	2.073	1.551	1.561	2.218	2.167	2.334	1.832	1.266	1.062	1.237	1.375
Mn		0.040	0.036	0.035	0.035	0.035	0.039	0.040	0.039	0.043	0.051	0.018	0.026	0.051	0.037	0.038	0.034	0.020	0.007	0.012	0.010
Mg		3.176	3.201	3.249	3.211	3.143	3.388	3.436	3.439	3.401	3.458	3.474	3.444	2.845	2.992	3.001	3.407	3.899	4.160	4.006	3.738
Σ M		6.272	6.318	6.230	6.200	6.178	6.225	6.291	6.240	6.295	6.383	5.835	5.849	5.951	6.018	6.207	6.093	6.011	6.066	6.065	5.933
Na		0.086	0.079	0.141	0.078	0.050	0.198	0.148	0.133	0.165	0.142	0.169	0.136	0.107	0.108	0.089	0.107	0.145	0.133	0.156	0.183
K		1.906	1.840	1.828	1.886	1.895	1.841	1.857	1.851	1.851	1.818	1.759	1.798	1.910	1.857	1.878	1.829	1.832	1.827	1.776	1.826
Σ I		1.992	1.920	1.969	1.964	1.945	2.039	2.006	1.985	2.016	1.961	1.927	1.934	2.017	1.965	1.967	1.936	1.977	1.960	1.933	2.010
F		0.090	0.056	0.043	0.070	0.047	0.180	0.155	0.065	0.017	0.073	0.202	0.123	0.048	0.122	0.145	0.087	0.145	0.040	0.371	0.322
Cl		0.002	0.005	0.006	0.008	0.010	0.005	0.008	0.007	0.005	0.006	0.011	0.002	0.009	0.000	0.000	0.007	0.021	0.017	0.018	0.021
OH		3.908	3.939	3.951	3.922	3.943	3.815	3.837	3.928	3.978	3.922	3.787	3.875	3.943	3.878	3.855	3.906	3.833	3.944	3.611	3.656
Σ A		4.000	4.000	4.000	4.000	4.000	4.000	4.000	4.000	4.000	4.001	4.000	4.000	4.000	4.000	4.000	4.000	3.999	4.001	4.000	3.999
Total cations		20.315	20.244	20.243	20.257	20.216	20.291	20.288	20.278	20.324	20.329	19.883	19.907	19.971	20.103	20.313	20.099	19.990	20.075	20.005	19.888
											calculated element ratios										
Fe.(Fe+Mg)		41.1	41.6	39.7	39.8	40.7	36.9	36.8	36.1	37.5	37.5	30.9	31.2	43.8	42.0	43.7	35.0	24.5	20.3	23.6	26.9
Mg.(Fe+Mg)		58.9	58.4	60.3	60.2	59.3	63.1	63.2	63.9	62.5	62.5	69.1	68.8	56.2	58.0	56.3	65.0	75.5	79.7	76.4	73.1

919

Table 4 – Main element oxide contents in wt% in selected feldspar grains from LIS syenites, by EPMA. $Fe_2O_3^T$ represents total iron (oxide) content. Numbers of cations in apfu calculated based on 8O, following guidance of Ribbe (1983)

spot	**LLD**	**1**	**2**	**3**	**4**	**5**	**6**	**7**	**8**	**9**	**10**	**11**	**12**	**13**	**14**	**15**	**16**	**17**	**18**	**19**	**20**
main element oxide contents in weight percent (wt%)																					
SiO_2	0.01	68.24	57.83	59.44	58.31	60.94	58.01	63.25	58.14	58.30	67.35	66.36	66.59	65.29	65.04	65.18	64.95	65.07	65.97	64.21	64.34
Al_2O_3	0.01	19.82	25.31	25.52	25.85	24.32	26.07	22.84	25.61	25.42	20.09	20.63	19.39	20.09	19.74	19.89	19.31	19.66	19.32	19.35	18.75
$Fe2O3^T$	0.01	0.03	0.45	0.37	0.46	0.18	0.47	0.15	0.49	0.41	0.04	0.07	0.10	0.19	0.12	0.20	0.39	0.09	0.27	0.21	0.10
MnO	0.01	<LLD	<LLD	0.01	<LLD	0.02	<LLD	0.01	<LLD	<LLD	0.02	0.02	<LLD	<LLD	<LLD	<LLD	0.01	0.04	<LLD	0.02	<LLD
MgO	0.01	<LLD	<LLD	0.01	0.03	0.28	0.03	<LLD	<LLD	0.02	<LLD	<LLD	<LLD	0.02	<LLD	<LLD	<LLD	<LLD	<LLD	<LLD	<LLD
CaO	0.01	0.29	7.18	7.24	7.88	5.94	8.13	3.90	7.70	7.63	0.59	1.46	0.46	1.44	0.97	0.77	0.56	0.63	0.47	0.38	0.37
Na_2O	0.01	10.67	5.89	6.77	6.41	7.53	6.47	8.35	6.88	5.86	10.50	9.71	7.03	6.28	5.64	5.25	4.57	4.77	5.09	2.30	3.31
K_2O	0.01	0.49	1.89	0.35	0.58	0.06	0.21	0.37	0.18	1.58	0.40	0.42	5.75	6.21	7.91	8.25	9.64	9.46	9.02	13.02	12.00
Total		99.54	98.55	99.71	99.52	99.27	99.39	98.87	99.00	99.22	98.99	98.67	99.32	99.52	99.42	99.54	99.43	99.72	100.14	99.49	98.87
numbers of cations in atoms per formula unit (apfu) on the basis of 8O																					
Si		2.990	2.630	2.660	2.620	2.720	2.610	2.820	2.620	2.640	2.970	2.940	2.980	2.940	2.940	2.950	2.960	2.950	2.970	2.950	2.970
Al		1.020	1.360	1.340	1.370	1.280	1.380	1.200	1.360	1.350	1.040	1.080	1.020	1.060	1.050	1.060	1.040	1.050	1.030	1.050	1.020
Fe		0.000	0.020	0.010	0.020	0.010	0.020	0.010	0.020	0.020	0.000	0.000	0.000	0.010	0.000	0.010	0.010	0.000	0.010	0.010	0.000
Σ T		4.010	4.010	4.010	4.010	4.010	4.010	4.030	4.000	4.010	4.010	4.020	4.000	4.010	3.990	4.020	4.010	4.000	4.010	4.010	3.990
Mn		0.000	0.000	0.000	0.000	0.000	0.000	0.000	0.000	0.000	0.000	0.000	0.000	0.000	0.000	0.000	0.000	0.000	0.000	0.000	0.000
Mg		0.000	0.000	0.000	0.000	0.020	0.000	0.000	0.000	0.000	0.000	0.000	0.000	0.000	0.000	0.000	0.000	0.000	0.000	0.000	0.000
Ca		0.010	0.350	0.350	0.380	0.280	0.390	0.190	0.370	0.370	0.030	0.070	0.020	0.070	0.050	0.040	0.030	0.030	0.020	0.020	0.020
Na		0.910	0.520	0.590	0.560	0.650	0.560	0.720	0.600	0.510	0.900	0.830	0.610	0.550	0.490	0.460	0.400	0.420	0.440	0.200	0.300
K		0.030	0.110	0.020	0.030	0.000	0.010	0.020	0.010	0.090	0.020	0.020	0.330	0.360	0.460	0.480	0.560	0.550	0.520	0.760	0.710
Σ M		0.950	0.980	0.960	0.970	0.950	0.960	0.930	0.980	0.970	0.950	0.920	0.960	0.980	1.000	0.980	0.990	1.000	0.980	0.980	1.030
Total cations		4.960	4.990	4.970	4.980	4.960	4.970	4.960	4.980	4.980	4.960	4.940	4.960	4.990	4.990	5.000	5.000	5.000	4.990	4.990	5.020
calculated feldspar endmember proportions (mol%)																					
Or		2.9	11.2	2.1	3.4	0.3	1.2	2.3	1.0	9.4	2.4	2.6	34.2	36.6	45.7	48.9	56.5	54.8	52.6	77.4	69.2
Ab		95.7	53.1	61.6	57.5	69.4	58.3	77.7	61.2	52.7	94.7	89.9	63.6	56.3	49.6	47.3	40.7	42.1	45.1	20.8	29.0
An		1.5	35.7	36.3	39.1	30.2	40.5	20.1	37.8	37.9	2.9	7.5	2.3	7.1	4.7	3.8	2.8	3.1	2.3	1.9	1.8
sum		100.0	100.0	100.0	100.0	100.0	100.0	100.0	100.0	100.0	100.0	100.0	100.0	100.0	100.0	100.0	100.0	100.0	100.0	100.0	100.0

Table 5 – Main element oxide contents in wt%, trace elements and rare-earth elements (REE) in parts per million (ppm; μg·g-1) in adakitic syenites from LIS, by ICP-MS (LOI gravimetric). $Fe_2O_3^T$ represents total iron (oxide) content.

sample	LLD	1	2	3	4	5	6	7	8	9	10	11	12	13	14	15
main element oxide contents in weight percent (wt%)																
Na_2O	0.01	4.80	4.78	4.35	4.29	4.21	4.50	4.26	4.24	3.68	4.24	6.41	5.58	4.37	3.93	4.04
K_2O	0.01	6.92	6.14	7.81	7.74	7.87	7.37	7.16	7.66	7.34	7.68	6.81	4.82	6.80	7.46	6.34
MgO	0.01	0.85	2.09	1.84	1.80	2.06	3.15	3.66	2.05	4.37	2.23	0.34	0.58	3.81	3.69	4.72
CaO	0.01	1.20	2.88	2.79	2.95	2.84	3.50	3.48	3.15	4.02	3.11	0.88	1.81	3.85	3.64	4.38
MnO	0.01	0.01	0.06	0.06	0.06	0.06	0.08	0.08	0.06	0.10	0.06	0.06	0.04	0.09	0.09	0.13
$Fe_2O_3^T$	0.01	1.98	4.32	3.76	3.73	3.76	4.78	5.25	4.01	6.19	4.02	2.16	2.03	5.52	5.42	7.43
Cr_2O_3	0.01	<0.01	<0.01	0.01	0.01	0.01	0.01	0.02	0.01	0.02	0.01	<0.01	<0.01	0.01	0.01	0.02
Al_2O_3	0.01	18.30	17.60	18.90	18.70	18.70	17.90	17.20	18.70	17.10	18.70	19.20	15.80	17.10	17.30	16.40
SiO_2	0.01	63.10	60.70	58.90	58.30	58.00	56.80	55.20	57.70	54.30	58.00	63.00	68.30	55.40	55.70	54.00
TiO_2	0.01	0.43	0.43	0.40	0.40	0.43	0.54	0.58	0.44	0.76	0.46	0.27	0.20	0.65	0.60	0.82
P_2O_5	0.01	0.41	0.46	0.46	0.47	0.53	0.72	0.78	0.52	1.20	0.56	0.02	0.10	1.00	0.95	1.22
LOI	0.01	1.58	1.03	0.78	0.98	0.76	0.70	0.80	0.71	1.08	0.66	0.96	0.87	1.19	0.97	0.98
Total		99.58	100.49	100.06	99.43	99.23	100.05	98.47	99.25	100.16	99.73	100.11	100.13	99.79	99.76	100.48
trace element contents in parts per million (ppm; μg·g-1)																
Ba	0.01	768	736	777	866	898	725	1050	989	750	922	31.1	459	872	921	569
Cr	0.01	20	20	30	30	40	100	150	50	110	40	10	20	90	80	120
Cs	0.01	4.35	5.10	9.17	8.25	8.37	10.20	13.90	9.06	8.10	7.47	10.50	0.82	7.11	6.62	21.50
Cu	0.01	3180	1080	67	79	92	177	238	84	233	106	39	50	120	304	303
Ga	0.01	15.0	14.6	13.2	13.1	12.8	13.5	13.9	14.4	13.4	12.8	18.2	13.3	14.6	12.2	15.8
Hf	0.01	5.5	5.1	3.1	2.9	2.9	3.5	4.0	3.0	2.7	2.8	7.5	5.6	4.3	1.4	4.5
Nb	0.01	15.6	14.3	13.0	12.2	11.6	16.3	16.4	13.3	15.5	11.8	48.5	13.8	18.6	10.8	20.9
Ni	0.01	24	35	37	37	43	59	78	32	75	34	13	20	71	68	62
Rb	0.01	260	206	223	213	215	232	252	230	233	210	337	148.5	244	206	275
Sn	0.01	2	1	1	1	1	1	1	1	1	1	2	1	1	1	1
Sr	0.01	522	710	898	1000	1000	836	1135	1115	768	1015	88.5	270	840	1090	504
Ta	0.01	0.8	0.8	0.6	0.6	0.5	0.7	0.8	0.6	0.6	0.7	3.6	0.9	0.9	0.4	1
Th	0.01	23.60	21.50	16.05	14.95	13.35	16.25	20.80	15.25	15.55	13.95	41.70	24.10	21.00	8.27	27.10
U	0.01	7.04	6.00	4.74	4.35	4.17	4.78	6.58	4.72	4.50	4.15	13.60	6.69	5.60	2.74	7.82
V	0.01	170	218	230	236	245	298	341	268	419	250	131	62	351	316	474
W	0.01	19	4	3	2	3	5	5	4	3	2	5	5	2	3	3
Y	0.01	11.80	13.20	9.20	8.60	8.70	11.10	12.30	9.70	14.10	9.10	15.90	15.50	15.60	11.90	18.50
Zr	0.01	220	196	128	118	111	145	166	119	110	118	240	202	175	52	189
rare-earth element (REE) contents in parts per million (ppm; μg·g-1)																
La	0.01	27.4	27.2	26.3	24.4	25.1	30.4	34.1	27.5	39.9	25.6	42.0	15.7	41.9	32.1	42.3
Ce	0.01	45.7	46.2	43.3	40.8	41.1	51.2	58.4	45.8	69.3	42.4	77.8	26.7	72.6	55.5	75.5
Pr	0.01	4.43	4.75	4.34	4.16	4.10	5.24	5.91	4.58	7.13	4.23	7.19	2.78	7.32	5.61	7.79
Nd	0.01	15.7	17.7	15.0	14.4	14.5	18.3	21.4	16.2	25.6	14.8	22.0	9.9	25.8	20.7	28.1
Pm																
Sm	0.01	3.09	3.80	3.00	2.70	2.93	3.71	4.42	3.08	5.32	2.96	4.17	2.47	5.29	4.25	5.40
Eu	0.01	0.75	0.88	0.69	0.74	0.78	0.83	0.95	0.85	1.12	0.80	0.29	0.55	1.07	1.02	1.17
Gd	0.01	2.59	3.04	2.25	2.25	2.40	2.99	3.31	2.50	4.03	2.34	3.11	2.43	4.06	3.32	4.30
Tb	0.01	0.34	0.41	0.32	0.30	0.31	0.40	0.41	0.34	0.50	0.30	0.50	0.39	0.51	0.42	0.57
Dy	0.01	1.90	2.40	1.65	1.47	1.60	2.13	2.33	1.88	2.78	1.56	2.93	2.37	2.77	2.27	3.14
Ho	0.01	0.42	0.47	0.37	0.30	0.34	0.41	0.47	0.37	0.53	0.35	0.60	0.56	0.61	0.45	0.64
Er	0.01	1.22	1.32	1.07	0.91	0.87	1.27	1.39	1.02	1.39	0.86	1.76	1.74	1.66	1.17	1.79
Tm	0.01	0.19	0.23	0.14	0.15	0.13	0.17	0.19	0.16	0.20	0.13	0.25	0.28	0.22	0.18	0.26
Yb	0.01	1.32	1.48	1.03	0.94	0.89	1.16	1.27	0.99	1.36	0.90	1.76	2.09	1.71	1.15	1.72
Lu	0.01	0.22	0.25	0.17	0.15	0.14	0.19	0.20	0.16	0.21	0.14	0.25	0.35	0.24	0.17	0.26

921

Supplementary Files

This is a list of supplementary files associated with this preprint. Click to download.

- MaartenXLSX.xlsx